Accepted Manuscript

Discovery of novel propargylamine-modified 4-aminoalkyl imidazole substituted pyrimidinylthiourea derivatives as multifunctional agents for the treatment of Alzheimer's disease

Yi-xiang Xu, Huan Wang, Xiao-kang Li, Sheng-nan Dong, Wen-wen Liu, Qi Gong, Tian-duan-yi Wang, Yun Tang, Jin Zhu, Jian Li, Hai-yan Zhang, Fei Mao

PII: S0223-5234(17)30628-1

DOI: 10.1016/j.ejmech.2017.08.025

Reference: EJMECH 9669

To appear in: *European Journal of Medicinal Chemistry*

Received Date: 11 February 2017

Revised Date: 7 August 2017

Accepted Date: 8 August 2017

Please cite this article as: Y.-x. Xu, H. Wang, X.-k. Li, S.-n. Dong, W.-w. Liu, Q. Gong, T.-d.-y. Wang, Y. Tang, J. Zhu, J. Li, H.-y. Zhang, F. Mao, Discovery of novel propargylamine-modified 4-aminoalkyl imidazole substituted pyrimidinylthiourea derivatives as multifunctional agents for the treatment of Alzheimer's disease, *European Journal of Medicinal Chemistry* (2017), doi: 10.1016/j.ejmech.2017.08.025.

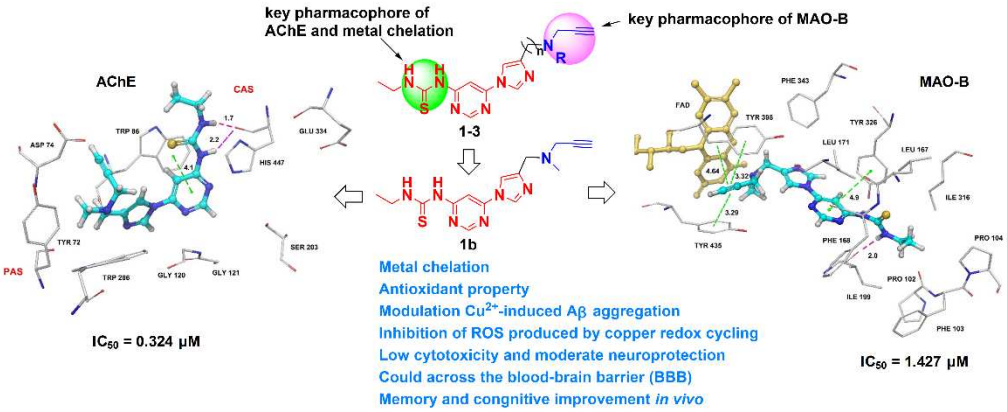

Metal chelation
Antioxidant property
Modulation Cu^{2+}-induced Aβ aggregation
Inhibition of ROS produced by copper redox cycling
Low cytotoxicity and moderate neuroprotection
Could across the blood-brain barrier (BBB)
Memory and congnitive improvement *in vivo*

Discovery of novel propargylamine-modified 4-aminoalkyl imidazole substituted pyrimidinylthiourea derivatives as multifunctional agents for the treatment of Alzheimer's Disease

Yi-xiang Xu[a,1], Huan Wang[b,c,1], Xiao-kang Li[a], Sheng-nan Dong[b], Wen-wen Liu[a], Qi Gong[b], Tian-duan-yi Wang[a], Yun Tang[a], Jin Zhu[a], Jian Li[a,*], Hai-yan Zhang[b,*], Fei Mao[a,*]

[a] Shanghai Key Laboratory of New Drug Design, School of Pharmacy, East China University of Science and Technology, 130 Mei Long Road, Shanghai 200237, China

[b] CAS Key Laboratory of Receptor Research, Shanghai Institute of Materia Medica, Chinese Academy of Sciences, 555 Zu Chong Zhi Road, Shanghai 201203, China

[c] University of Chinese Academy of Science, No.19A Yuquan Road, Beijing 100049, China

[1] These authors contributed equally to this work.

[*] To whom correspondence should be addressed maofei@ecust.edu.cn, hzhang@simm.ac.cn, jianli@ecust.edu.cn.

ABSTRACT:

A series of novel propargylamine-modified pyrimidinylthiourea derivatives (**1-3**) were designed and synthesized as multifunctional agents for Alzheimer's disease (AD) therapy, and their potential was evaluated through various biological experiments. Among these derivatives, compound **1b** displayed good selective inhibitory activity against AChE (*vs* BuChE, IC_{50} = 0.324 μM, SI > 123) and MAO-B (*vs* MAO-A, IC_{50} = 1.427 μM, SI > 35). Molecular docking study showed that the pyrimidinylthiourea moiety of **1b** could bind to the catalytic active site (CAS) of AChE, and the propargylamine moiety interacted directly with the flavin adenine dinucleotide (FAD) of MAO-B. Moreover, **1b** demonstrated mild antioxidant ability, good copper chelating property, effective inhibitory activity against Cu^{2+}-induced $A\beta_{1-42}$ aggregation, moderate neuroprotection, low cytotoxicity, and appropriate blood−brain barrier (BBB) permeability *in vitro* and was capable of ameliorating scopolamine-induced cognitive impairment in mice. These results indicated that **1b** has the potential to be a multifunctional candidate for the treatment of Alzheimer's disease.

Keywords: Multifunctional agents, AChE inhibitors, MAO-B inhibitors, Metal chelating agents, Alzheimer's disease.

1. Introduction

Alzheimer's disease (AD) is a progressive and chronic neurodegenerative disorder characterized by memory loss and cognitive impairments [1,2]. The number of dementia patients has reached over 46 million by 2015 and is expected to triple by 2050 [3]. Due to its complex etiology, the pathogenesis has not been fully elucidated, and there have been various pathogenesis hypotheses for AD, such as cholinergic hypothesis [4], amyloid cascade hypothesis [5,6], oxidative stress hypothesis [7], and metal dishomeostasis hypothesis [8,9].

Among these hypotheses, the cholinergic deficit hypothesis has been generally accepted by most researchers. This theory suggests that AD patients' learning-memory and cognitive ability dysfunction is closely related to the low acetylcholine (ACh) levels in brain [10,11]. Thus, strengthening the central cholinergic activity and increasing the level of ACh in the brain, for example, by inhibiting the activity of acetylcholinesterase (AChE) have been considered to be effective approaches for the treatment of AD [12,13]. Currently, the clinical first-line drugs for the treatment of AD are mainly AChE inhibitors such as donepezil, rivastigmine, galantamine, and huperzine A (Hup A, approved by CFDA) [14,15]. However, these drugs only improve the memory and cognitive abilities of AD patients but fail to achieve a radical cure [16,17].

Many studies have found that monoamine oxidase (MAO) also plays a very important role in the pathogenesis of AD because the increase of MAO in the brain may result in a cascade of biochemical events leading to neuronal dysfunction [18,19]. Monoamine oxidases (MAOs) are flavin adenine dinucleotide (FAD)-containing enzymes that are responsible for the oxidative deamination of endogenous and exogenous monoamine substances. MAOs have two functional isozymic forms, namely, MAO-A and MAO-B [20]. MAO-A inhibitors are used as clinical antidepressants and anti-anxiety agents, whereas MAO-B inhibitors are applied to treat neurodegenerative disorders such as AD and Parkinson's diseases (PD) [21,22]. According to previous studies [23,24], the activities of MAO-B in the brain and blood platelets of AD patients were increased, while high expression levels of MAO-B

could cause the high level of free radicals that played a key role in the pathogenesis of AD. MAO-B inhibitors can reduce the oxidative stress response and protect the nerve cells from oxidative damage and neurotoxicity, and therefore, MAO-B has been another important target for the treatment of AD [25,26]. Among the MAO inhibitors, selegiline, an irreversible and selective MAO-B inhibitor, has been reported as a potential anti-AD agent due to its neuroprotective property in cellular and animal models of AD [27].

In addition, recent studies have revealed that the high levels and dysregulation of biometal ions were closely implicated in the pathogenesis of AD [8,9,28]. Metal ions such as Cu^{2+}, Zn^{2+} and Fe^{2+} have been shown to facilitate Aβ aggregation, leading to the generation of toxic Aβ oligomers [29]. In particular, redox-active Cu (I/II) and Fe (II/III) are implicated in the generation of reactive oxygen species (ROS) leading to an increased oxidative stress [30-33]. Biometal chelators, especially Cu^{2+} chelators, not only reduce the metal-induced Aβ aggregation but also reduce the level of ROS produced by the redox metal and metal-Aβ complex [33,34]. Therefore, biometal chelators have been considered as a potential therapeutic approach for AD. Furthermore, neurotoxic ROS and oxidative damage of neuronal cells are also associated with AD, so that compounds with antioxidant activities are beneficial for the treatment of AD [35,36].

Taking the complex pathogenesis of AD and the impotency of single-target drugs into consideration, the development of multi-target-directed ligands (MTDLs) has been proposed to be an effective approach for the treatment of AD [37,38]. Considering that ChEs and MAOs are important targets for the treatment of AD, some researchers have devoted their efforts to finding multifunctional agents that target both ChEs and MAOs. For example, Ladostigil (**Fig. 1**), generated by joining the carbamate moiety of rivastigmine and indolamine moiety of rasagiline, shows bifunctional inhibitory activities of MAOs and ChEs in a single molecule, and presently, it is in a Phase III clinical trial for the treatment of mild cognitive impairment (MCI). This indicates that the combination of ChEs inhibitor and MAOs inhibitor is a promising therapeutic method for AD [39-41].

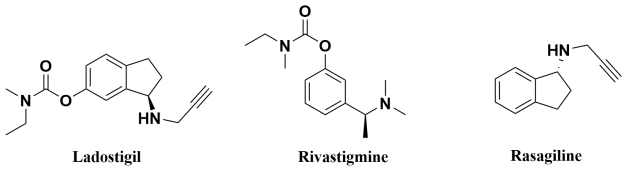

Fig. 1. Chemical structures of ladostigil, rivastigmine and rasagiline

Inspired by the MTDLs strategy, we designed and synthesized a series of novel pyrimidinylthiourea derivatives as multifunctional agents for the potential treatment of AD in our previous work. These derivatives exhibited potent inhibition and good selectivity toward AChE, specific metal-chelating ability, mild antioxidant effects, low cytotoxicity, and good blood–brain barrier (BBB) permeability and could improve memory and cognitive function of scopolamine-induced cognitive impairment mice [42]. In this work, we combined the imidazole-substituted pyrimidinylthiourea moiety (AChE inhibitor's pharmacophore) and the propargylamine moiety (MAO-B inhibitor's pharmacophore) of selegiline [27] or pargyline [43] into a single molecule (**Fig. 2**). These derivatives showed good inhibition for both AChE and MAO-B, as well as the abilities of metal-chelating, modulating metal induced Aβ aggregation, free radical scavenging, mild antioxidant properties, neuroprotection and low cytotoxicity.

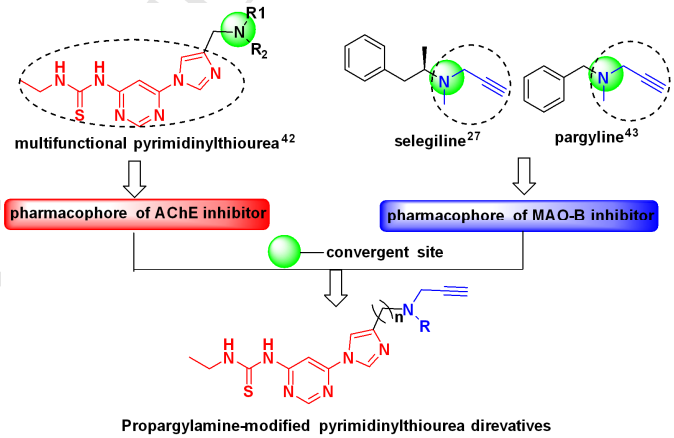

Fig. 2. Design strategy for the new series of propargylamine-modified pyrimidinylthiourea derivatives.

2. Results and discussion

2.1. Design and synthesis

To study the SAR of new compounds and find the optimal compound, structural

modifications were performed. First, "R" at the *N*-atom of propargylamine was modified with hydrogen, methyl, ethyl, propyl, butyl, acetyl, benzyl, cyanomethyl and propargyl to study the effect of different sizes of substitution on multiple functions (compounds **1a-i**). Next, to obtain the optimal linker between imidazole ring and propargylamine, the length of carbon spacer ("n") was changed from one to three or a ring (compounds **2a-d**, **3a-b**, and **1j**). The synthesis of propargylamine-modified pyrimidinylthiourea derivatives (**1-3**) was carried out following the sequence of reactions depicted in **Scheme 1**. The nucleophilic substitution reaction of imidazole derivatives (**4a-c**) and 4-amino-6-chloropyrimidine in the presence of inorganic base (K_2CO_3 or Cs_2CO_3) provided intermediates **5a-c**, followed by the condensation reaction with ethylisothiocyanate in the presence of NaH affording the key intermediates **6a-c**. The target compounds **1a-b** and **1j** were obtained by reductive amination of intermediate **6a** with diverse propargylamines in the presence of $NaBH_3(CN)$. Next, the nucleophilic substitution reaction of **1a** with haloalkane or acetylchloride in the presence of Et_3N provided compounds **1c-i**. To obtain compounds **2a-d** and **3a-b**, the intermediates **7b-c** were synthesized by the bromination reaction of **6b-c** with PBr_3. Then, the nucleophilic substitution of **7b-c** with propargylamine or *N*-methyipropargaylamine afforded the target compounds **2a-b** and **3a-b**. Similarly, the nucleophilic substitution reaction of **2a** with haloalkane in the presence of Et_3N furnished the target compounds **2c-d**.

The details of the synthetic procedures and structural characterizations of target compounds (^{1}H NMR, ^{13}C NMR, and HRMS spectroscopy) and intermediates (^{1}H NMR) are described in the experimental section. The purities of all target compounds were determined by HPLC.

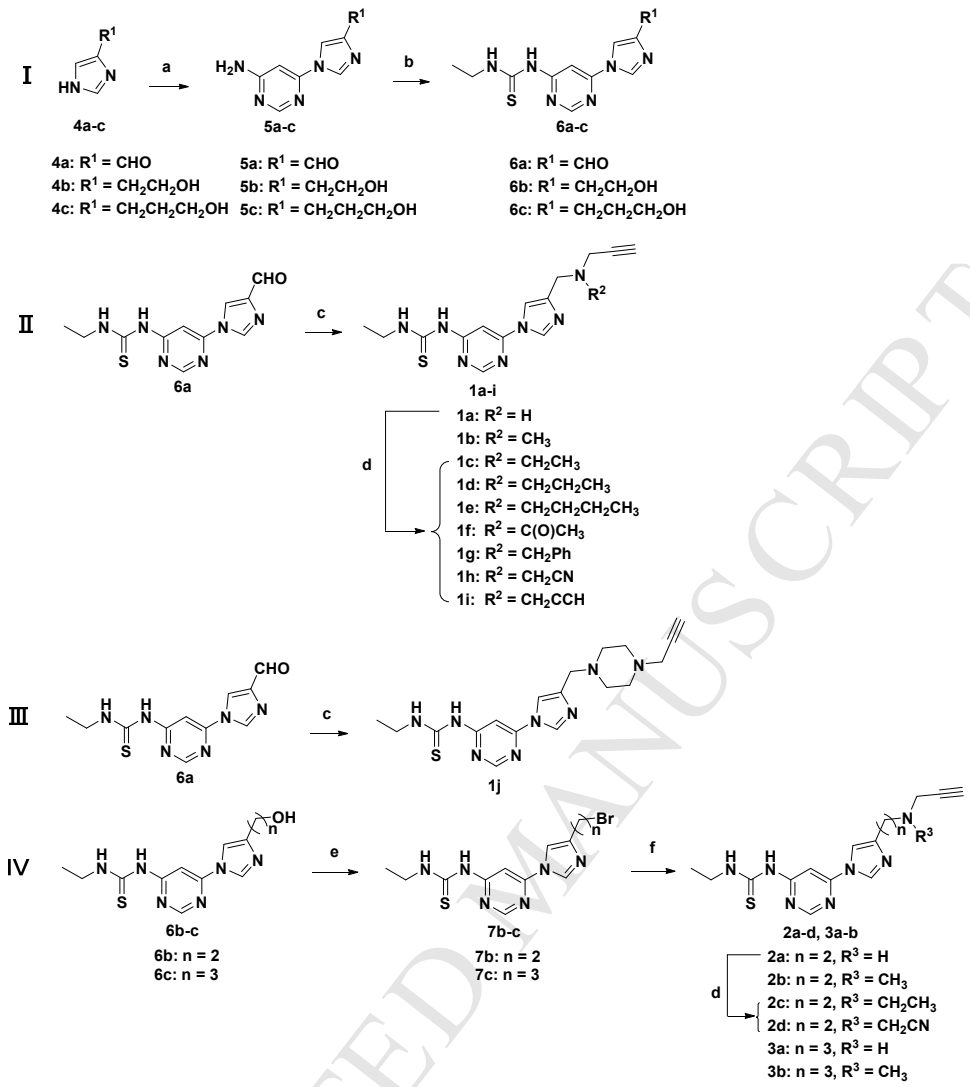

Scheme 1. Synthetic route to compounds **1a-j**, **2a-d** and **3a-b**. Reagents and conditions: (a) (i) for **5a**: 4-amino-6-chloropyrimidine, K_2CO_3, DMF, 100 °C, 12 h; (ii) for **5b-c**: 4-amino-6-chloropyrimidine, Cs_2CO_3, DMF, 140 °C, 12 h; (b) CH_3CH_2NCS, NaH, DMF, rt, 0.5 h; (c) 2-Propynylamine, *N*-methylpropargylamine or 1-(prop-2-yn-1-yl)piperazine, $NaBH_3(CN)$, MeOH:DCE = 1:1 (v:v), AcOH, rt, 12 h; (d) (i) for **1c-e** and **1g-i**: RX, acetonitrile, Et_3N, reflux, 12 h; (ii) for **1f**: acetyl chloride, DCM, Et_3N, rt; (e) PBr_3, DCM, rt, overnight; (f) 2-Propynylamine or N-methylpropargylamine, K_2CO_3, rt, overnight.

2.2. Biological activity

2.2.1. In vitro inhibition studies of AChE and BuChE

To evaluate the therapeutic potential of these propargylamine-modified pyrimidinylthiourea derivatives for AD, compounds **1a−j**, **2a−d**, and **3a−b** were

assayed against rat ChE (rChE) by the modified method of Ellman et al. [44], using huperzine A (Hup A) as a reference compound. As shown in **Table 1**, all of our target compounds exhibited desirable inhibitory activity to rAChE and poor inhibitory activity against rBuChE (SI> 30), indicating that these derivatives were selective AChE inhibitors. Examination of the IC_{50} values of compounds **1a-i** shows that unsubstituted compound **1a** (IC_{50} = 0.354 μM for AChE) and methyl substituted compound **1b** (IC_{50} = 0.324 μM for AChE) exhibited higher activity than compounds **1c-i** (IC_{50} > 0.4 μM for AChE) with larger substitutions. This suggested that the size of the substitution at the *N*-atom of propargylamine has a moderate influence on the AChE inhibitory activity, and the appropriate substituents at the *N*-atom of propargylamine appeared to be methyl and hydrogen. Then, the influence of the linker length to AChE inhibitory activity was also studied; however, compounds **1a-b**, **2a-b** and **3a-b** exhibited similar inhibitory activities for AChE. The inhibitory activity result of compound **1j** shows that the use of the piperazine ring as the linker led to a decrease in AChE inhibitory activity.

Table 1.

Structures, rAChE and rBuChE inhibitory activities, and selectivity index for rAChE of the target compounds.

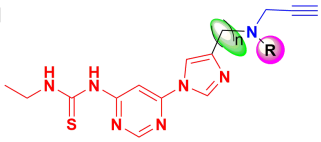

Compd	**n**	**R**	IC_{50} (μM)[a] for rAChE	IC_{50} (μM)[a] for rBuChE (Inhibition at 40 μM)	SI[b]
1a	1	H	0.354 ± 0.057	>40 (15.24%)	>113
1b	1	CH_3	0.324 ± 0.022	>40 (12.59%)	>123
1c	1	CH_2CH_3	0.482 ± 0.019	>40 (10.49%)	>83
1d	1	$(CH_2)_2CH_3$	0.485 ± 0.025	>40 (7.75%)	>83
1e	1	$(CH_2)_3CH_3$	0.675 ± 0.072	>40 (13.42%)	>59
1f	1	$C(O)CH_3$	0.515 ± 0.070	>40 (5.15%)	>78

1g	1	CH_2Ph	0.585 ± 0.012	>40 (9.28%)	>68
1h	1	CH_2CN	0.707 ± 0.044	>40 (5.48%)	>57
1i	1	CH_2CCH	0.718 ± 0.034	>40 (4.97%)	>56
2a	2	H	0.228 ± 0.027	>40 (8.73%)	>175
2b	2	CH_3	0.392 ± 0.037	>40 (8.91%)	>102
2c	2	CH_2CH_3	1.337 ± 0.184	>40 (2.44%)	>30
2d	2	CH_2CN	0.597 ± 0.011	>40 (3.02%)	>67
3a	3	H	0.381 ± 0.052	>40 (12.74%)	>105
3b	3	CH_3	0.459 ± 0.052	>40 (6.70%)	>87
1j	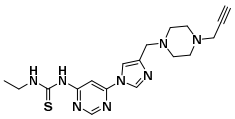		0.482 ± 0.029	>40 (7.30%)	>83
Hup A			0.098 ± 0.016	36.4 ±1.838	>371

[a]Results are expressed as the mean ± SD of at least three independent experiments. [b]Selectivity index for AChE is defined as IC_{50}(rBuChE)/IC_{50}(rAChE).

2.2.2. In vitro inhibition studies of MAOs

To confirm the multipotent biological functions of these new compounds, inhibitory activities against the recombinant human MAOs (hMAO-A and hMAO-B) were determined using clorgyline and pargyline as the reference compounds, respectively. The corresponding IC_{50} values or the percentage of inhibition at 50 μM are shown in **Table 2**. The data showed that only a fraction of the tested compounds could effectively inhibit MAO-A or MAO-B. Among the synthesized compounds, **1b** was the most potent selective inhibitor against MAO-B (IC_{50} = 1.472 μM, SI > 35), and **1a** exhibited the highest potency for both MAO-A and MAO-B (IC_{50} = 4.327 μM and 5.236 μM, respectively). The other compounds, except **1a-b, 2b** and **3b**, showed weak activities with IC_{50} values over 50 μM. This result suggested that the enlargement of the substitution at the *N*-atom of propargylamine dramatically decrease the inhibitory activity for MAOs. For unsubstituted compounds (**1a**, **2a** and **3a**), once the linker length changed from 1 to 3 carbon atoms, the inhibitory activities for MAO-A and MAO-B decreased sharply (**1a**: IC_{50} = 4.327 μM for MAO-A, IC_{50} =

5.236 μM for MAO-B; **2a** and **3a**: IC_{50} > 50 mM for both MAO-A and MAO-B); for *N*-methyl substituted compounds (**1b**, **2b** and **3b**), the linker length affected the selectivity toward MAO-A and MAO-B: compound **2b** with a 2 carbon atoms-long linker exhibited inhibitory activities for both MAO-A and MAO-B, whereas **1b** and **3b**, with 1 and 3 carbon atoms-long linkers, respectively, were good selective inhibitors against MAO-B. This meant that the selectivity of the compounds towards MAO-A and MAO-B is closely related to the length of the linker.

Table 2.

Structures, hMAO-A and hMAO-B inhibitory activities, and selectivity index for hMAO-B of the target compounds.

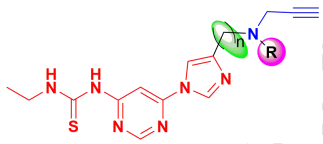

Compd	n	R	IC_{50} (μM)[a] for hMAO-A (Inhibition at 50 μM)	IC_{50} (μM)[a] for hMAO-B (Inhibition at 50 μM)	SI[b]	ORAC[c]
1a	1	H	4.327 ± 0.299	5.236 ± 0.527	0.826	1.175 ± 0.061
1b	1	CH_3	>50 (20.22%)	1.427 ± 0.272	>35	1.126 ± 0.015
1c	1	CH_2CH_3	>50 (6.71%)	>50 (35.12%)		1.383 ± 0.061
1d	1	$(CH_2)_2CH_3$	>50 (1.76%)	>50 (24.31%)		0.448 ± 0.222
1e	1	$(CH_2)_3CH_3$	>50 (2.43%)	>50 (20.11%)		0.238 ± 0.013
1f	1	$C(O)CH_3$	>50 (4.83%)	>50 (1.17%)		1.167 ± 0.035
1g	1	CH_2Ph	>50 (17.82%)	>50 (18.44%)		n.t.
1h	1	CH_2CN	>50 (2.01%)	>50 (15.35%)		0.494 ± 0.031
1i	1	CH_2CCH	>50 (15.47%)	>50 (42.11%)		0.585 ± 0.070
2a	2	H	>50 (54.24%)	>50 (19.23%)		1.272 ± 0.053
2b	2	CH_3	9.003 ± 0.982	12.435 ± 1.082	0.724	1.243 ± 0.016
2c	2	CH_2CH_3	>50 (13.03%)	>50 (49.4%)		n.t.
2d	2	CH_2CN	>50 (13.92%)	>50 (24.94%)		0.556 ± 0.029
3a	3	H	>50 (31.39%)	>50 (36.59%)		0.186 ± 0.004

3b	3	CH_3	>50 (63.77%)	3.229 ± 0.557	>15	0.447 ± 0.169
1j		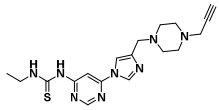	>50 (9.22%)	>50 (13.29%)		1.028 ± 0.061
Clorgyline			12.850 ± 0.495 (nM)	n.t.[d]		n.t.
Pargyline			n.t.	0.188 ± 0.061		n.t.

[a]Results are expressed as the mean ± SD of at least two experiments. [b]Selectivity index for MAO-B is defined as IC_{50}(MAO-A)/IC_{50}(MAO-B). [c]The mean ± SD of three independent experiments. Data are expressed as μmol of Trolox equivalent/μmol of tested compounds. [d]No test.

2.2.3. Free oxygen radical scavenging ability

Given that reactive radical species have been identified to be closely related to AD [45], compounds that can decrease reactive radical species may exert potential therapeutic effects. The oxygen radical absorbance capacity assay (ORAC-FL) was performed to evaluate the antioxidant activity of these target compounds. This assay used fluorescein as the fluorescent probe, AAPH (2,2'-azobis-(amidinopropane)dihydrochloride) as the peroxyl radical inducer, and the water-soluble analogue of vitamin E, Trolox, as the standard [46,47]. ORAC values were expressed as Trolox equivalents calculated from the antioxidant of tested compounds *vs* Trolox (the ORAC value of Trolox = 1.00). The results (**Table 2**) indicated that half of the tested compounds exhibited mild antioxidant ability with ORAC values of 1.028−1.383. The modification of the "R" substituent at the *N*-position and changes in the length of the linker obviously affected the antioxidant activity (**1c** *vs* **1d-e**; **1a** and **2a** *vs* **3a**): unsubstituted and small-size substituent compounds with 1−2 carbon atoms linker length exhibited relatively good antioxidant activity (ORAC values > 1), whereas the rest of the tested compounds displayed weak antioxidant activity (ORAC values < 1). Compound **1c** displayed the best antioxidant activity, with an ORAC value of 1.383.

2.2.4. Metal chelating effect

Based on above biological evaluation results, compound **1b** was the most promising compound with excellent multiple functions (IC_{50} = 0.324 μM for AChE; IC_{50} = 1.472 μM for MAO-B; ORAC value of 1.126 for antioxidant activity). Therefore, compound **1b** was chosen for further biological evaluation.

The metal chelating activity of compound **1b** with copper, zinc, and iron was measured by UV−vis spectroscopy assay. In our previous work [42], we found that thiourea fragment played the key role in the generation of the metal chelating action, and the pyrimidinylthiourea derivatives could selectively chelate Cu^{2+}. As expected, when $CuCl_2$ was added to the solution of **1b**, the maximum absorption decreased dramatically at 290 nm (**Fig. 3**), demonstrating the formation of **1b**−Cu^{2+} complexes, while only vague optical shift and maximum absorption fluctuation were observed when $FeSO_4$, $FeCl_3$, and $ZnCl_2$ were added, indicating that compound **1b** has better selectivity towards Cu^{2+}.

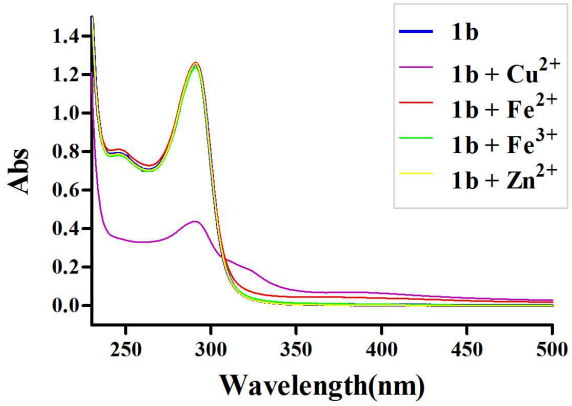

Fig. 3. UV spectra of compound **1b** (40 μM) alone and in the presence of $CuCl_2$ (20 μM), $FeSO_4$ (20 μM), $FeCl_3$ (20 μM), or $ZnCl_2$ (20 μM) in buffer (20 mM HEPES, 150 mM NaCl, pH 7.4).

2.2.5. Inhibition of ROS produced by copper redox cycling

Many researchers have found that redox-active metal ions were closely involved in the high oxidative stress caused by ROS [31], which is a proposed pathogenesis of AD. To evaluate the ability of compound **1b** to inhibit the ROS produced by Cu(II)-related redox, the model of the Cu-ascorbate redox system described by Faller and co-workers was used (**Fig. 4A**) [48], using the metal chelator

ethylenediaminetetraacetic acid (EDTA) as the positive control. Hydroxyl radicals (OH·), produced by copper redox cycling in the presence of ascorbate, could oxidize coumarin-3-carboxylic acid (CCA) to fluorescent 7-hydroxy CCA so that the fluorescence values could indicate the amount of OH·. As shown in **Fig. 4B**, the fluorescence value of the copper-ascorbate system increased steadily with time and reached a plateau at approximately 800 s. However, the value changed little when compound **1b** was coincubated with the Cu-ascorbate system and was the same as the value of the sample without Cu(II). The result showed that compound **1b** could halt copper redox cycling.

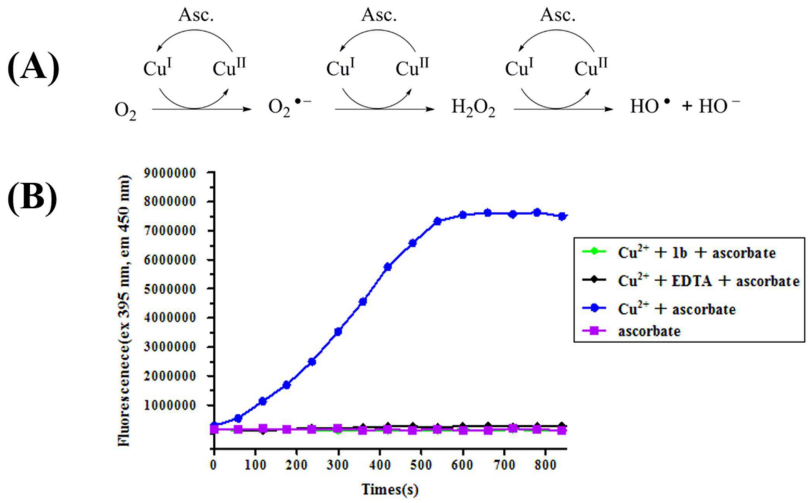

Fig. 4. (A) Oxygen reduction by copper redox cycling in the presence of ascorbate. (B) Fluorescence intensity of the copper-ascorbate-**1b**, copper-ascorbate-EDTA, copper-ascorbate, and ascorbate alone systems. CCA (50 μM) and ascorbate (150 μM) were incubated in each system. [Cu^{2+}] = 5 μM, [**1b**] = [EDTA] = 15 μM. PBS buffer (20 mM KH_2PO_4, 150 mM NaCl); N = 3; pH = 7.4; 37 °C.

2.2.6. Dot blot assay and TEM assay

A dot blot assay was performed to evaluate the modulation of metal-induced A*β* aggregation by compound **1b**, and a transmission electron microscopy (TEM) assay was then performed to examine the morphological changes of the A*β* species. In the dot blot assay, the samples were probed by the A11 antibody to determine the oligomeric A*β*, and total A*β* was detected by 6E10 as the loading control. A representative scan graph and a statistical histogram are shown in **Fig. 5A**; the gray

density of the spots is proportional to the level of the Aβ oligomerization. The results showed that Aβ aggregated spontaneously, and compound **1b** showed no effect on the Aβ self-aggregation after 24 h incubation. Epigallocatechin gallate (EGCG) was tested as the positive control. A thioflavine T (ThT) fluorescence assay was performed to verify this result (**Fig. S1**, *Supporting Information*). The dot blot assay showed that Cu^{2+} could accelerate Aβ aggregation and that this process was significantly inhibited by compound **1b**.

The TEM experiment showed that the aggregation of Aβ in the presence of Cu^{2+} produced more fibrils than self-induced Aβ aggregation (**Fig. 5B**, images 2 and 3). As expected, fewer Aβ fibrils were detected when compound **1b** and clioquinol (CQ) were incubated with the sample after incubation for 24 h at 37 °C (**Fig. 5B**, images 4 and 5), indicating that **1b** can efficiently inhibit Cu^{2+}-induced Aβ aggregation.

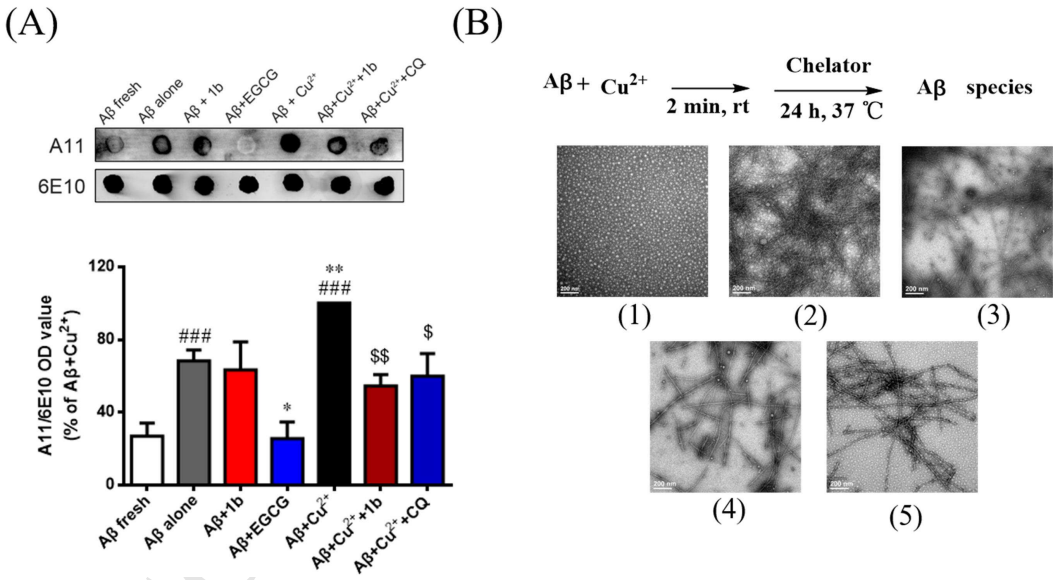

Fig. 5. Inhibition of compound on Cu^{2+}-induced Aβ_{1-42} aggregation. (A) Scan and bar graph of the dot blot assay. Aggregated Aβ was detected by A11 antibody, and total Aβ was probed by 6E10 antibody. Data are shown as the mean ± SEM, $^{###}p < 0.001$ *vs* Aβ fresh, $^{*}p < 0.05$, $^{**}p < 0.01$ *vs* Aβ alone, $^{\$}p < 0.05$, $^{\$\$}p < 0.01$ *vs* Aβ + Cu^{2+}, N = 4. (B) TEM image analysis of copper induced Aβ_{1-42} aggregation studies ([Aβ_{1-42}] = [Cu^{2+}] = 25 μM, [compd] = 50 μM; HEPES (20 μM) and NaCl (150 μM); pH 6.6; 37 °C). (1) fresh Aβ_{1-42}, (2) Aβ_{1-42} + Cu^{2+}, (3) Aβ_{1-42} alone, (4) Aβ_{1-42} + Cu^{2+} + **1b**, (5) Aβ_{1-42} + Cu^{2+} + CQ.

2.2.7. MTT Assay

To investigate the safety of the propargylamine-modified 4-aminoalkyl imidazole substituted pyrimidinylthiourea derivatives, the cytotoxicity of compound **1b** on rat primary cortical neuron (PCN) was studied using a 3-(4,5-dimethylthiazol-2-yl)-2,5-diphenyltetrazolium bromide (MTT) assay and donepezil (Don) tested as the reference. The result is depicted in **Fig. 6A**. Similar to Don, compound **1b** exhibited no cytotoxicity at concentrations of 10 μM and 30 μM after incubation for 24 h. When the concentration increased to a relatively high level of 100 μM, **1b** showed a significant but mild neurotoxicity ($^{*}p < 0.05$ *vs* Ctrl) compared to Don ($^{***}p < 0.001$ *vs* Ctrl). Therefore, the MTT assay showed that compound **1b** was weakly cytotoxic.

Neurotoxicity, neuronal damage and neuronal cell apoptosis caused by the toxic A*β* oligomer are important causes of AD. To determine whether compound **1b** can protect neuronal cells from toxic A*β* species, cell viability experiments were conducted using PCNs. EGCG (inhibitor of A*β* self-aggregation) and CQ (inhibitor of Cu^{2+}-induced A*β* aggregation) were tested as positive controls. The results are shown in **Fig. 6B**. Incubation of PCNs with A*β* in the presence of Cu^{2+} caused higher cytotoxicity than the A*β* alone group ($^{*}p < 0.05$). Compared to the A*β* + Cu^{2+} group, compound **1b**, like CQ, could protect the PCNs from Cu^{2+}-induced A*β* neurotoxicity, leading to a significant increase in cell viability ($^{\$\$}p < 0.01$). Moreover, compound **1b** could not interact with A*β* directly to restrain the cytotoxicity produced by the A*β*-self aggregates. These results were highly consistent with the results of the dot blot assay.

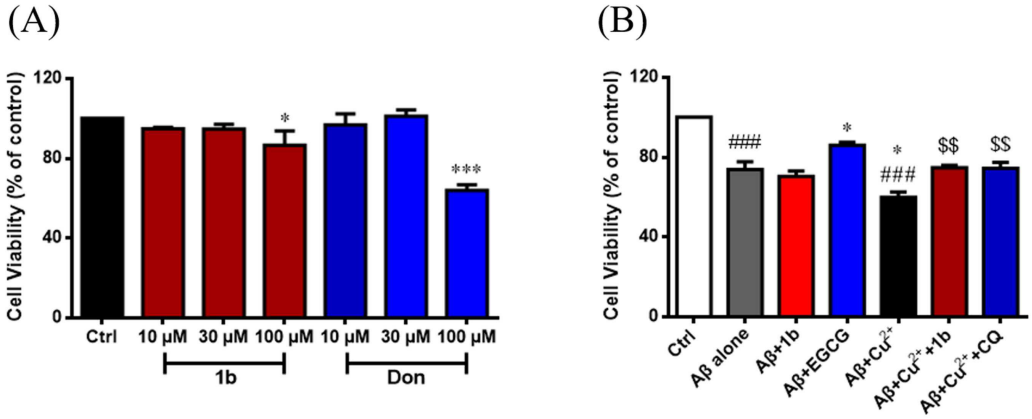

Fig. 6. (A) Cell viability of primary cortical neurons exposed to compound **1b** and Don at di▪erent concentrations (range 10−100 μM) for 24 h. Vehicle-treated cells were used as controls. The results are expressed as the percentage of viable cells observed after treatment with compound *vs* vehicle-treated cells (100%) and are shown as the mean ± SEM; $^{*}p < 0.05$, $^{***}p < 0.001$ *vs* Ctrl, N = 3; (B) Protection of compound **1b** from Cu^{2+}-induced $A\beta_{1\text{-}42}$ neurotoxicity. Data are shown as the mean ± SEM; N = 3. Experimental conditions: $[A\beta_{1-42}] = [Cu^{2+}] = 1$ μM, [compd] = 2 μM. $^{\#\#\#}p < 0.001$ *vs* Ctrl, $^{*}p < 0.05$ *vs* Aβ alone, $^{\$\$}p < 0.01$ *vs* Aβ + Cu^{2+}.

2.2.8. In vitro blood−brain barrier permeation assay

To evaluate the target compounds' BBB penetrability, we carried out the parallel artificial membrane permeation assay (PAMPA) [49]. First, to validate the assay, the values of permeability (P_e) of 13 commercial drugs were determined and compared to the reported values. A plot of the experimental data versus reference values gave a strong linear correlation, P_e (exp.) = 0.947P_e (bibl.) – 0.8152 (R^2 = 0.9651, **Fig. S2**, *Supporting Information*). Based on this equation and the limit established by Di et al. for blood−brain barrier permeation, we concluded that compounds with P_e values greater than 3.08×10^{-6} cm s^{-1} could cross the blood−brain barrier by passive permeation (CNS+). P_e values from 1.13×10^{-6} cm s^{-1} to 3.08×10^{-6} cm s^{-1} were classified as "CNS±", uncertain BBB permeation. The results of PAMPA-BBB assay are presented in **Table 3**. It can be observed that compounds **1b**, **2a-b** and **3a-b** could cross the BBB, whereas compound **1a** exhibited uncertain BBB permeation (CNS±). It can also be seen that the compounds' BBB permeation ability is related to the length of the linker (**3b** > **2b** > **1b**).

Table 3.

Permeability results ($P_e\times10^{-6}$ cm s^{-1}) from the PAMPA-BBB assay for compounds **1a-b**, **2a-b** and **3a-b** and their prediction of BBB penetration.

Compd	P_e (10^{-6} cm s^{-1})[a]	prediction[b]
1a	2.78 ± 0.12	CNS±
1b	3.16 ± 0.10	CNS+

2a	3.24 ± 0.08	CNS+
2b	3.33 ± 0.12	CNS+
3a	3.26 ± 0.21	CNS+
3b	3.98 ± 0.09	CNS+

[a]Values are expressed as the mean ± SD of at least three independent experiments. [b]Compounds with $P_e > 3.08 \times 10^{-6}$ cm s^{-1} could cross the BBB by passive di□usion (CNS+). Compounds with $P_e < 1.13 \times 10^{-6}$ cm s^{-1} could not cross the BBB (CNS−), and compounds with 1.13×10^{-6} cm $s^{-1} < P_e < 3.08 \times 10^{-6}$ cm s^{-1} show uncertain BBB permeation (CNS±).

*2.2.9. Improvement of cognition in scopolamine-induced dementia mice by **1b**.*

To analyze the *in vivo* effect of compound **1b** on cognitive impairment, scopolamine-induced cognitive performance deficits in the channel water maze were employed, with huperzine A (Hup A) as a positive control. As shown in **Fig. 7**, mice treated with scopolamine (4.5 mg/kg, i.p.) required longer time to find the platform (escape latency) and committed more errors (entering no-exit paths) than those of the control group ($^{###}p < 0.001$) in the water maze task. Compound **1b·HCl**, administered to mice orally at a dose of 30 mg/kg, could ameliorate scopolamine-induced learning and memory deficits, with the mice in this group showing shorter escape latency and less frequent errors compare to the scopolamine group ($^{*}p < 0.05$). Therefore, compound **1b·HCl** has the potential to be a lead anti-AD agent due to its symptomatic improvement effect in the AD mice model.

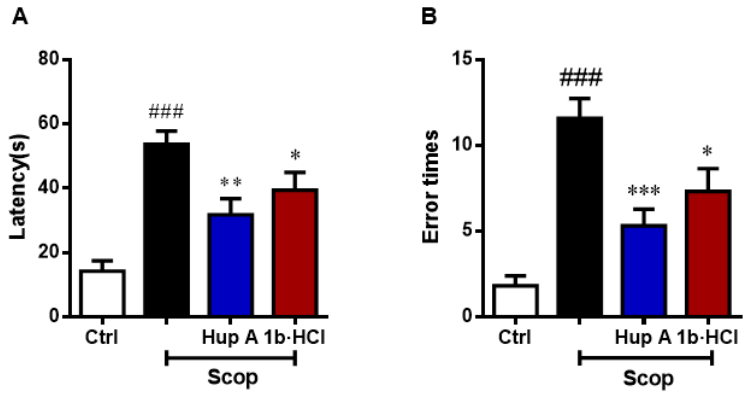

Fig. 7. Effect of compound **1b·HCl** (30 mg/kg) on scopolamine-induced cognitive deficit mice, with Hup A (0.1 mg/kg) as positive control: (A) Escape latency of mice

in water maze; (B) Number of errors of mice in water maze. Data are shown as the mean ± SEM: $^{###}p < 0.001$ *vs* Ctrl, $^{*}p < 0.05$, $^{**}p < 0.01$, $^{***}p < 0.001$ *vs* Scop, N = 16. Ctrl: control; Scop: scopolamine; HupA: huperzine A.

2.3. Molecular docking studies of AChE and MAO-B

To confirm the rationality of compound design and explore the interaction mode of target compounds with enzymes, molecular docking simulations of **1b** with mice AChE (mAChE) and human MAO-B (hMAO-B) were performed using Glide in Schrödinger software. The X-ray crystallographic structure of mAChE complexed with tacrine (PDB code 5EIE), and human MAO-B complexed with 7-(3-chlorobenzyloxy)-4-formylcoumarin (PDB code 2V60) were obtained from the Protein Data Bank. As shown in **Fig. 8A**, compound **1b** interacts with the CAS of AChE via π-π interactions and hydrogen bond interactions. The two strong hydrogen bonds between the thiourea-NH (1.7 Å) and carbonyl of His 447 (2.2 Å) may play an important role in the positioning and the stabilization of the ligand inside the CAS. Moreover, its pyrimidine ring could interact with Trp86 via face-to-face π-π stacking interaction with the distance of 4.1 Å. The results also validated the hypothesis that the thiourea and pyrimidine fragments were key groups for maintaining the AChE activity [42].

Examination of **Fig. 8B** shows that the propargylamine group of **1b** has a favorable fit into the substrate cavity of the enzyme, oriented to the flavin adenine dinucleotide (FAD) cofactor in close proximity (4.64 Å), and is properly adopted between Tyr398 (3.32 Å) and Tyr435 (3.29 Å), forming face-to-face cation-π stacking interactions in a “sandwich” form. Additionally, the face-to-edge π-π stacking interaction (4.9 Å) between the pyrimidine ring and Trp326 and the hydrogen bond (2.0 Å) between thiourea-NH and carbonyl of Ile199 could stabilize the ligand in the catalysis gorge of the enzyme. Moreover, the ethyl group of thiourea may be embedded into the hydrophobic pocket in the entrance cavity formed by Pro104, Phe103, Pro102, Ile199, Ile316, Leu167 and Phe168.

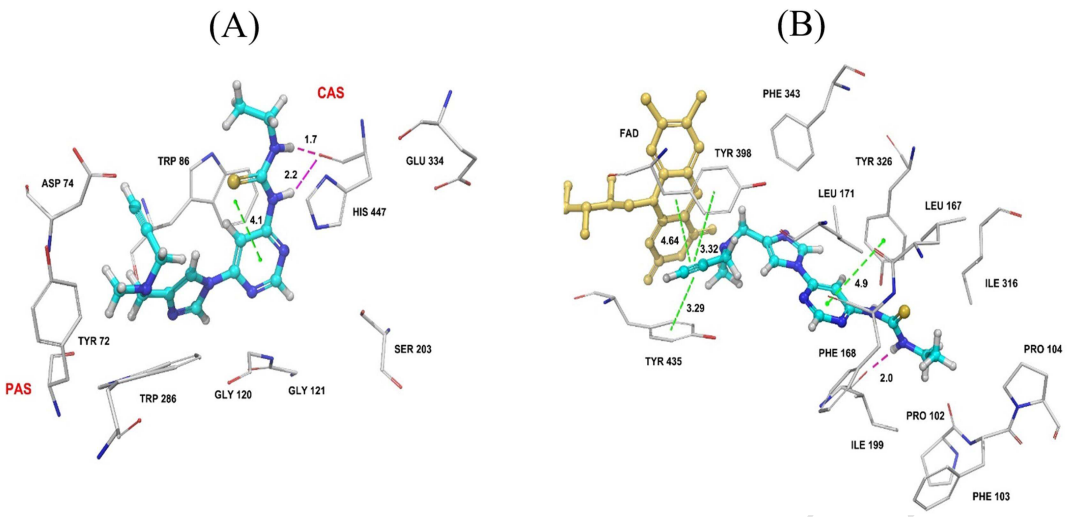

Fig. 8. (A) 3D docking model of compound **1b** with mAChE. (B) 3D docking model of compound **1b** with hMAO-B. Compound **1b** is illustrated using blue sticks, and the FAD cofactor is depicted using yellow sticks. π-π stacking interactions are highlighted by green lines, and hydrogen bonds are shown with purple dash lines.

3. Conclusions

Multi-target-directed ligands (MTDLs), aiming to simultaneously target multiple pathological processes involved in the neurodegenerative cascade, have been developed as effective agents for the treatment of Alzheimer's disease. Our previous studies obtained the pyrimidinylthiourea derivatives as MTDLs with ChE inhibitory activity, specific metal-chelating ability and mild antioxidant effect. In the present study, by introducing the MAO-B inhibitor's pharmacophore propargylamine into the pyrimidinylthiourea scaffold, a series of novel propargylamine-modified 4-aminoalkyl imidazole substituted pyrimidinylthiourea derivatives have been designed, synthesized, and evaluated as potential multifunctional anti-AD agents. The activities of all synthesized compounds were evaluated against rAChE, rBuChE, hMAO-A(B), and antioxidant ability. The SAR studies revealed that the size of the substitution at the *N*-atom of propargylamine strongly influences the AChE and MAOs inhibition and the antioxidant activity. Among all derivatives, compound **1b** displayed good selective inhibitory activities against AChE (IC_{50} = 0.324 μM, SI > 123) and MAO-B (IC_{50} = 1.427 μM, SI > 35) and demonstrated mild antioxidant ability (ORAC = 1.126), good copper chelating property, effective inhibitory activity against

Cu^{2+}-induced Aβ_{1-42} aggregation, low cytotoxicity and moderate neuroprotection against Cu^{2+}-induced Aβ_{1-42} neurotoxicity in primary cultured cortical neurons and appropriate blood−brain barrier (BBB) permeability *in vitro*. The molecular docking simulations of **1b** with mAChE and hMAO-B also confirmed the rationality of our design strategy. Furthermore, compound **1b·HCl** could improve the memory and cognitive function of Scop-induced dementia mice. Taken together, these results showed that the new compound **1b** can be considered a potential multifunctional agent for AD therapy.

4. Experimental section

4.1. Chemistry

4.1.1. General methods

All common reagents and solvents were obtained from commercial suppliers and used without purification. Reaction progress was monitored using analytical thin layer chromatography (TLC), HSGF 254 (150−200 μm thickness; Yantai Huiyou Co., China), and the spots were detected under UV light (254 nm). Melting points were measured in capillary tubes on a SGWX−4 melting point apparatus without correction. ^{1}H NMR and ^{13}C NMR spectra were recorded on a Bruker AMX 400 and AMX 500 spectrometer in DMSO-d_6, CD_3COCD_3 or CD_3OD with TMS as internal standard. Chemical shifts were reported in parts per million (ppm, δ) downfield from tetramethylsilane. Proton coupling patterns were described as singlet (s), doublet (d), triplet (t), quartet (q), multiplet (m), and broad (br). High-resolution mass spectra (HRMS) were obtained by electric ionization (EI) and electrospray ionization (ESI) using a Waters GCT Premie and Waters LCT. All target compounds were purified to ≥ 95% purity as determined by an Agilent 1100 with a quaternary pump and diode array detector (DAD). The eluent was CH_3OH:H_2O = 80:20 (v:v), flow rate was 0.5 mL/min, and the relative purity of each compound calculated at 254 nm.

*4.1.2. General synthetic procedure for **5a-c***

A mixture of imidazole derivatives (**4a-c**, 10 mmol), 4-amino-6-chloropyrimidine (1.30 g, 10 mmol), and K_2CO_3 (2.07 g, 15 mmol, for **5a**) or Cs_2CO_3 (3.91 g, 12 mmol, for **5b-c**) was stirred in DMF (20 mL) at 100 °C (for **5a**)

or at 140 °C (for **5b-c**) for 12 h. Water (100 mL) was then added. The mixture was extracted with EtOAc (3 × 50 mL). The organic layer was separated and dried over Na_2SO_4. Removal of the solvents produced a residue which was purified using column chromatography and eluted with a mixture of MeOH:CH_2Cl_2 (1:30, v:v) to afford **5a-c**.

4.1.2.1. 1-(6-Aminopyrimidin-4-yl)-1H-imidazole-4-carbaldehyde (***5a***) [42]. White solid, 46% yield. ^{1}H NMR (400 MHz, DMSO-d_6) δ 9.83 (s, 1H), 8.70 (s, 1H), 8.64 (s, 1H), 8.37 (s, 1H), 7.35 (s, 2H), 6.72 (s, 1H).

4.1.2.2. 2-(1-(6-Aminopyrimidin-4-yl)-1H-imidazol-4-yl)ethan-1-ol (***5b***). White solid, 58% yield. ^{1}H NMR (400 MHz, DMSO-d_6) δ 8.33 (s, 1H), 8.29 (s, 1H), 7.54 (s, 1H), 7.16 (s, 2H), 6.50 (s, 1H), 4.64 (br, 1H), 3.70–3.60 (m, 2H), 2.66 (t, J = 6.9 Hz, 2H).

4.1.2.3. 3-(1-(6-Aminopyrimidin-4-yl)-1H-imidazol-4-yl)propan-1-ol (***5c***). White solid, 41% yield. ^{1}H NMR (400 MHz, DMSO-d_6) δ 8.33 (d, J = 1.1 Hz, 1H), 8.29 (s, 1H), 7.50 (s, 1H), 7.13 (s, 2H), 6.50 (d, J = 0.7 Hz, 1H), 4.47 (t, J = 5.2 Hz, 1H), 3.50 – 3.38 (m, 2H), 2.59–2.51 (m, 2H), 1.81–1.69 (m, 2H).

*4.1.3. General synthetic procedure for **6a-c***

NaH (60% dispersion in mineral oil, 96 mg, 2.4 mmol) was added to a solution of corresponding intermediates **5a-c** (2 mmol) in DMF (10 mL). The solution was stirred for 5 min, and then, ethyl isothiocyanate (174 mg, 2 mmol) was added. The reaction mixture was stirred at room temperature for 0.5 h. Water was added, and the mixture was extracted with EtOAc (3 × 60 mL). The organic layer was separated and dried over Na_2SO_4. Removal of the solvents produced a residue, which was purified using column chromatograph and eluted with a mixture of MeOH:CH_2Cl_2 (1:40, v:v) to afford corresponding intermediates **6a-c**.

4.1.3.1. 1-Ethyl-3-(6-(4-formyl-1H-imidazol-1-yl)pyrimidin-4-yl)thiourea (***6a***) [42]. White solid, 60% yield. ^{1}H NMR (400 MHz, DMSO-d_6) δ 11.13 (t, J = 5.1 Hz, 1H), 11.10 (s, 1H), 9.88 (s, 1H), 8.83 (s, 1H), 8.61 (s, 2H), 7.42 (s, 1H), 3.72–3.57 (m, 2H), 1.23 (t, J = 7.2 Hz, 3H).

4.1.3.2. 1-Ethyl-3-(6-(4-(2-hydroxyethyl)-1H-imidazol-1-yl)pyrimidin-4-yl)

thiourea (***6b***). White solid, 41% yield. ^{1}H NMR (400 MHz, CD_3OD) δ 8.69 (d, J = 0.9 Hz, 1H), 8.52 (d, J = 1.2 Hz, 1H), 7.64 (s, 1H), 6.98 (d, J = 0.9 Hz, 1H), 3.84 (t, J = 6.7 Hz, 2H), 3.74 (q, J = 7.3 Hz, 2H), 2.82 (t, J = 6.7 Hz, 2H), 1.31 (t, J = 7.3 Hz, 3H).

4.1.3.3. 1-ethyl-3-(6-(4-(3-hydroxypropyl)-1H-imidazol-1-yl)pyrimidin-4-yl) thiourea (***6c***). White solid, 35% yield. ^{1}H NMR (400 MHz, DMSO-d_6) δ 11.19 (t, J = 5.0 Hz, 1H), 10.92 (s, 1H), 8.74 (s, 1H), 8.35 (s, 1H), 7.42 (s, 1H), 7.25 (s, 1H), 4.48 (t, J = 5.2 Hz, 1H), 3.70–3.59 (m, 2H), 3.49–3.40 (m, 2H), 2.56 (t, J = 7.5 Hz, 2H), 1.81–1.71 (m, 2H), 1.22 (t, J = 7.2 Hz, 3H).

*4.1.4. General synthetic procedure for **1a-b** and **1j***

Propargylamine (0.75 mmol) and AcOH (0.75 mmol) corresponding to a solution of compound **6a** (138 mg, 0.5 mmol) in MeOH:DCE = 1:1 were added. The solution was stirred for 10 min, and then, $NaBH_3(CN)$ (62.8 mg, 1 mmol) was added. The mixture was stirred at room temperature for 12 h, and the solvent was evaporated to dryness under reduced pressure. The residue was purified on a silica gel column using mixtures of MeOH:CH_2Cl_2 as the eluent, obtaining the target compounds **1a-b** and **1j**.

4.1.4.1. 1-Ethyl-3-(6-(4-((prop-2-yn-1-ylamino)methyl)-1H-imidazol-1-yl) pyrimidin-4-yl)thiourea (***1a***). The corresponding propargylamine was 2-Propynylamine. White solid, 53% yield. Mp 166–167 °C; ^{1}H NMR (400 MHz, CD_3OD) δ 8.71 (d, J = 1.0 Hz, 1H), 8.55 (d, J = 1.2 Hz, 1H), 7.76 (s, 1H), 7.02 (d, J = 1.0 Hz, 1H), 3.86 (s, 2H), 3.74 (q, J = 7.3 Hz, 2H), 3.46 (d, J = 2.5 Hz, 2H), 2.67 (t, J = 2.5 Hz, 1H), 1.31 (t, J = 7.3 Hz, 3H). ^{13}C NMR (125 MHz, DMSO-d_6) δ 179.18, 159.95, 157.33, 154.44, 143.17, 134.64, 112.55, 94.29, 82.74, 73.79, 45.03, 39.69, 36.83, 13.65. HRMS (EI): m/z calcd $C_{14}H_{17}N_7S$ (M^+) 315.1266, found 315.1269. HPLC purity: 98.0%.

4.1.4.2. 1-Ethyl-3-(6-(4-((methyl(prop-2-yn-1-yl)amino)methyl)-1H-imidazol-1-yl) pyrimidin-4-yl)thiourea (***1b***). The corresponding propargylamine was *N*-methylpropargylamine. White solid, 30% yield. Mp 183–184 °C; ^{1}H NMR (400 MHz, CD_3OD) δ 8.71 (d, J = 1.0 Hz, 1H), 8.54 (d, J = 1.3 Hz, 1H), 7.78 (s, 1H), 7.02 (d, J = 1.0 Hz, 1H), 3.74 (q, J = 7.3 Hz, 2H), 3.65 (s, 2H), 3.39 (d, J = 2.4 Hz, 2H),

2.71 (t, *J* = 2.4 Hz, 1H), 2.38 (s, 3H), 1.31 (t, *J* = 7.3 Hz, 3H). ^{13}C NMR (125 MHz, DMSO-d_6) δ 179.17, 159.94, 157.33, 154.39, 141.15, 134.70, 113.88, 94.46, 79.13, 75.84, 52.34, 44.53, 41.15, 39.69, 13.65. HRMS (EI): *m*/*z* calcd $C_{15}H_{19}N_7S$ (M^+) 329.1423, found 329.1425. HPLC purity: 99.1%.

4.1.4.3. 1-Ethyl-3-(6-(4-((4-(prop-2-yn-1-yl)piperazin-1-yl)methyl)-1H-imidazol -1-yl)pyrimidin-4-yl)thiourea (***1j***). The corresponding propargylamine was 1-(prop-2-yn-1-yl)piperazine. Yellow solid, 28% yield. Mp 160−162 °C; ^{1}H NMR (400 MHz, CD_3COCD_3) δ 11.35 (br, 1H), 9.79 (s, 1H), 8.71 (s, 1H), 8.36 (d, *J* = 1.2 Hz, 1H), 7.61 (s, 1H), 7.32 (s, 1H), 3.82–3.61 (m, 2H), 3.51 (s, 2H), 3.27 (d, *J* = 2.4 Hz, 2H), 2.69 (t, *J* = 2.4 Hz, 1H), 2.55 (br, 8H), 1.29 (t, *J* = 7.2 Hz, 3H). ^{13}C NMR (100 MHz, DMSO-d_6) δ 179.18, 159.95, 157.34, 154.40, 140.94, 134.62, 113.86, 94.44, 79.36, 75.67, 54.95, 52.33, 51.05, 45.96, 39.73, 13.68. HRMS (EI): *m*/*z* calcd $C_{18}H_{24}N_8S$ (M^+) 384.1845, found 384.1847. HPLC purity: 96.1%.

4.1.5. General synthetic procedure for ***1c-i***

To a solution of compound **1a** (158 mg, 0.5 mmol) in CH_3CN (8 mL), corresponding RX (0.55 mmol), Et_3N (101 mg, 1 mmol), and a catalytic amount of KI were added. The reaction mixture was refluxed for 12 h, and the solvent was evaporated to dryness under reduced pressure. The residue was purified on a silica gel column using mixtures of MeOH:CH_2Cl_2 as the eluent, affording the target compounds **1c-i**.

4.1.5.1. 1-Ethyl-3-(6-(4-((ethyl(prop-2-yn-1-yl)amino)methyl)-1H-imidazol-1-yl) pyrimidin-4-yl)thiourea (***1c***). Iodoethane was used as the corresponding RX. White solid, 27% yield. Mp 163−164 °C; ^{1}H NMR (400 MHz, DMSO-d_6) δ 11.18 (br, 1H), 10.91 (s, 1H), 8.75 (s, 1H), 8.39 (s, 1H), 7.54 (s, 1H), 7.28 (s, 1H), 3.68–3.60 (m, 2H), 3.58 (s, 2H), 3.38 (s, 2H), 3.14 (s, 1H), 2.59–2.52 (m, 2H), 1.22 (t, *J* = 7.2 Hz, 3H), 1.03 (t, *J* = 7.0 Hz, 3H). ^{13}C NMR (100 MHz, DMSO-d_6) δ 179.18, 159.95, 157.35, 154.37, 141.10, 134.75, 113.90, 94.43, 78.86, 75.77, 50.07, 46.45, 40.77, 39.73, 13.68, 12.47. HRMS (EI): *m*/*z* calcd $C_{16}H_{21}N_7S$ (M^+) 343.1579, found 343.1583. HPLC purity: 98.0%.

4.1.5.2. 1-Ethyl-3-(6-(4-((prop-2-yn-1-yl(propyl)amino)methyl)-1H-imidazol-1-yl)

pyrimidin-4-yl)thiourea (***1d***). 1-Iodopropane was used as the corresponding RX. White solid, 30% yield. Mp 158−159 °C; ^{1}H NMR (400 MHz, CD_3OD) δ 8.71 (d, J = 1.0 Hz, 1H), 8.53 (d, J = 1.3 Hz, 1H), 7.75 (s, 1H), 7.02 (d, J = 1.0 Hz, 1H), 3.74 (q, J = 7.3 Hz, 2H), 3.69 (s, 2H), 3.43 (d, J = 2.4 Hz, 2H), 2.65 (t, J = 2.4 Hz, 1H), 2.61–2.51 (m, 2H), 1.62–1.51 (m, 2H), 1.31 (t, J = 7.3 Hz, 3H), 0.93 (t, J = 7.4 Hz, 3H). ^{13}C NMR (125 MHz, DMSO-d_6) δ 179.17, 159.92, 157.31, 154.36, 141.51, 134.65, 113.60, 94.38, 79.14, 75.51, 54.39, 50.37, 41.28, 39.69, 20.05, 13.63, 11.70. HRMS (EI): *m*/*z* calcd $C_{17}H_{23}N_7S$ (M^+) 357.1736, found 357.1734. HPLC purity: 98.9%.

4.1.5.3. 1-(6-(4-((Butyl(prop-2-yn-1-yl)amino)methyl)-1H-imidazol-1-yl) pyrimidin-4-yl)-3-ethylthiourea (***1e***). 1-Iodobutane was used as the corresponding RX. Faint yellow solid, 28% yield. Mp 112−114 °C; ^{1}H NMR (400 MHz, CD_3OD) δ 8.71 (d, J = 0.9 Hz, 1H), 8.53 (d, J = 1.2 Hz, 1H), 7.76 (s, 1H), 7.03 (d, J = 0.9 Hz, 1H), 3.74 (q, J = 7.3 Hz, 2H), 3.70 (s, 2H), 3.44 (d, J = 2.4 Hz, 2H), 2.66 (t, J = 2.4 Hz, 1H), 2.63–2.58 (m, 2H), 1.58–1.47 (m, 2H), 1.41–1.34 (m, 2H), 1.31 (t, J = 7.3 Hz, 3H), 0.94 (t, J = 7.3 Hz, 3H). ^{13}C NMR (100 MHz, DMSO-d_6) δ 179.18, 159.95, 157.34, 154.37, 141.44, 134.69, 113.68, 94.38, 79.08, 75.63, 52.07, 50.37, 41.29, 39.73, 28.97, 19.94, 13.88, 13.67. HRMS (EI): *m*/*z* calcd $C_{18}H_{25}N_7S$ (M^+) 371.1892, found 371.1895. HPLC purity: 96.6%.

4.1.5.4. N-((1-(6-(3-Ethylthioureido)pyrimidin-4-yl)-1H-imidazol-4-yl) methyl)-N- (prop-2-yn-1-yl)acetamide (***1f***). Reagents used were compound **1a** (158 mg, 0.5 mmol), acetyl chloride (47 mg, 0.75 mmol), Et_3N (101 mg, 1 mmol), DCM (5 mL), rt, 12 h. Purification involved the use of MeOH/CH_2Cl_2 as eluent. Compound **1f**: white solid, 45% yield. Mp 197−199 °C; ^{1}H NMR (400 MHz, CD_3OD) δ 8.73 (8.72) (d, J = 0.8 Hz, 1H), 8.58 (8.55) (d, J = 1.1 Hz, 1H), 7.88 (7.79) (s, 1H), 7.04 (7.02) (d, J = 0.8 Hz, 1H), 4.70 (4.65) (s, 2H), 4.25 (d, J = 2.4 Hz, 2H), 3.75 (q, J = 7.3 Hz, 2H), 2.81 (2.66) (t, J = 2.3 Hz, 1H), 2.30 (2.25) (s, 3H), 1.33 (t, J = 7.3 Hz, 3H). ^{13}C NMR (125 MHz, DMSO-d_6) δ 179.16, 169.65 (169.57), 159.94, 157.34, 154.31, 140.33 (139.86), 135.42 (134.84), 113.78 (113.63), 94.61 (94.46), 79.97 (79.61), 74.83 (73.86), 44.46 (41.92), 39.69 (s), 37.48 (33.55), 21.49 (21.38), 13.63. HRMS (ESI):

m/*z* calcd $C_{16}H_{19}N_7OS$ $[M+H]^+$ 358.1405, found 358.1448. HPLC purity: 98.5%.

4.1.5.5. 1-(6-(4-((Benzyl(prop-2-yn-1-yl)amino)methyl)-1H-imidazol-1-yl) pyrimidin-4-yl)-3-ethylthiourea (***1g***). (Bromomethyl)benzene was used as the corresponding RX. White solid, 48% yield. Mp 146−147 °C; ^{1}H NMR (400 MHz, CD_3OD) δ 8.71 (d, J = 0.9 Hz, 1H), 8.55 (d, J = 1.3 Hz, 1H), 7.78 (s, 1H), 7.40 (d, J = 7.0 Hz, 2H), 7.31 (t, J = 7.3 Hz, 2H), 7.25 (t, J = 7.2 Hz, 1H), 7.03 (d, J = 0.9 Hz, 1H), 3.84–3.62 (m, 6H), 3.33 (s, 2H), 2.71 (t, J = 2.3 Hz, 1H), 1.31 (t, J = 7.3 Hz, 3H). ^{13}C NMR (125 MHz, DMSO-d_6) δ 179.17, 159.92, 157.31, 154.34, 141.23, 138.51, 134.79, 128.62, 128.23, 127.03, 113.80, 94.46, 78.77, 76.10, 56.60, 49.90, 41.05, 39.69, 13.64. HRMS (EI): *m*/*z* calcd $C_{21}H_{23}N_7S$ (M^+) 405.1736, found 405.1737. HPLC purity: 98.0%.

4.1.5.6. 1-(6-(4-(((Cyanomethyl)(prop-2-yn-1-yl)amino)methyl)-1H-imidazol-1-yl) pyrimidin-4-yl)-3-ethylthiourea (***1h***). 2-Bromoacetonitrile was used as the corresponding RX. Yellow solid, 36% yield. Mp 151−152 °C; ^{1}H NMR (400 MHz, CD_3OD) δ 8.72 (d, J = 0.9 Hz, 1H), 8.57 (d, J = 1.2 Hz, 1H), 7.84 (s, 1H), 7.02 (d, J = 0.9 Hz, 1H), 3.82–3.77 (m, 4H), 3.74 (q, J = 7.3 Hz, 2H), 3.51 (d, J = 2.4 Hz, 2H), 2.79 (t, J = 2.4 Hz, 1H), 1.31 (t, J = 7.3 Hz, 3H). ^{13}C NMR (125 MHz, DMSO-d_6) δ 179.16, 159.95, 157.35, 154.32, 139.49, 135.12, 116.01, 114.71, 94.56, 78.45, 76.67, 49.67, 42.22, 40.77, 39.69, 13.64. HRMS (ESI): *m*/*z* calcd $C_{16}H_{18}N_8S$ $[M+H]^+$ 355.1409, found 355.1454. HPLC purity: 97.1%.

4.1.5.7. 1-(6-(4-((Di(prop-2-yn-1-yl)amino)methyl)-1H-imidazol-1-yl) pyrimidin -4-yl)-3-ethylthiourea (***1i***). 3-Bromoprop-1-yne was used as the corresponding RX. White solid, 36% yield. Mp 151−153 °C; ^{1}H NMR (400 MHz, DMSO-d_6) δ 11.17 (t, J = 5.2 Hz, 1H), 10.91 (s, 1H), 8.73 (s, 1H), 8.40 (s, 1H), 7.56 (s, 1H), 7.27 (s, 1H), 3.67 – 3.60 (m, 2H), 3.59 (s, 2H), 3.41 (d, J = 1.8 Hz, 4H), 3.20 (s, 2H), 1.22 (t, J = 7.2 Hz, 3H).^{13}C NMR (100 MHz, DMSO-d_6) δ 179.17, 159.96, 157.36, 154.35, 140.50, 134.93, 114.23, 94.52, 79.09, 75.90, 49.57, 41.28, 39.73, 13.69. HRMS (EI): *m*/*z* calcd $C_{17}H_{19}N_7S$ (M^+) 353.1423, found 353.1402. HPLC purity: 98.9%.

*4.1.6. General synthetic procedure for **7b-c***

PBr_3 (541 mg, 2 mmol) was dropped to a solution of compounds **6b-c** (2 mmol)

in DCM (30 mL). The mixture was stirred at room temperature overnight, and the solvent was evaporated to dryness under reduced pressure. The residue was purified on a silica gel column using mixtures of MeOH:CH_2Cl_2 as the eluent to afford the target compounds **7b-c**.

4.1.6.1. 1-(6-(4-(2-Bromoethyl)-1H-imidazol-1-yl)pyrimidin-4-yl)-3-ethyl thiourea (***7b***). White solid, 28% yield. ^{1}H NMR (400 MHz, DMSO-d_6) δ 11.19 (t, J = 5.6 Hz, 1H), 10.98 (s, 1H), 8.75 (s, 1H), 8.40 (s, 1H), 7.61 (s, 1H), 7.27 (s, 1H), 3.76 (t, J = 6.9 Hz, 2H), 3.69–3.58 (m, 2H), 3.11 (t, J = 6.9 Hz, 2H), 1.22 (t, J = 7.2 Hz, 3H).

4.1.6.2. 1-(6-(4-(3-Bromopropyl)-1H-imidazol-1-yl)pyrimidin-4-yl)-3-ethyl thiourea (***7c***). White solid, 30% yield. ^{1}H NMR (400 MHz, DMSO-d_6) δ 11.27 (s, 1H), 11.03 (t, J = 5.4 Hz, 1H), 9.88 (s, 1H), 8.88 (s, 1H), 8.00 (d, J = 1.3 Hz, 1H), 7.46 (s, 1H), 4.36 (t, J = 7.3 Hz, 2H), 3.69–3.58 (m, 2H), 3.02 (t, J = 7.0 Hz, 2H), 2.63–2.54 (m, 2H), 1.21 (t, J = 7.2 Hz, 3H).

*4.1.7. General synthetic procedure for **2a-b** and **3a-b***

A mixture of **7b-c** (0.5 mmol) and K_2CO_3 (172 mg, 1.25 mmol) was stirred overnight in 2-propynylamine or *N*-methylpropargylamine (1 mL) at room temperature. The mixture was then evaporated to dryness under reduced pressure. The residue was purified on a silica gel column using mixtures of MeOH:CH_2Cl_2 as the eluent to afford the corresponding compounds **2a-b** and **3a-b**.

4.1.7.1. 1-Ethyl-3-(6-(4-(2-(prop-2-yn-1-yl)amino)ethyl)-1H-imidazol-1-yl) pyrimidin-4-yl)thiourea (***2a***). Yellow solid, 70% yield. Mp 159−160 °C; ^{1}H NMR (400 MHz, CD_3OD) δ 8.70 (d, J = 0.9 Hz, 1H), 8.52 (d, J = 1.3 Hz, 1H), 7.63 (s, 1H), 6.98 (d, J = 0.9 Hz, 1H), 3.74 (q, J = 7.3 Hz, 2H), 3.44 (d, J = 2.5 Hz, 2H), 3.00 (t, J = 7.2 Hz, 2H), 2.81 (t, J = 7.2 Hz, 2H), 2.62 (t, J = 2.5 Hz, 1H), 1.31 (t, J = 7.3 Hz, 3H). ^{13}C NMR (100 MHz, DMSO-d_6) δ 179.20, 159.95, 157.31, 154.44, 142.94, 134.47, 112.06, 94.17, 83.09, 73.53, 47.37, 39.73, 37.32, 28.04, 13.69. HRMS (EI): *m*/*z* calcd $C_{15}H_{19}N_7S$ (M^+) 329.1423, found 329.1424. HPLC purity: 99.0%.

4.1.7.2. 1-Ethyl-3-(6-(4-(2-(methyl(prop-2-yn-1-yl)amino)ethyl)-1H-imidazol -1-yl)pyrimidin-4-yl) thiourea (***2b***). Yellow solid, 68% yield. Mp 162−164 °C; ^{1}H

NMR (400 MHz, CD_3OD) δ 8.70 (d, J = 0.9 Hz, 1H), 8.51 (d, J = 1.3 Hz, 1H), 7.65 (s, 1H), 6.98 (d, J = 0.9 Hz, 1H), 3.74 (q, J = 7.3 Hz, 2H), 3.44 (d, J = 2.4 Hz, 2H), 2.87–2.77 (m, 4H), 2.69 (t, J = 2.4 Hz, 1H), 2.40 (s, 3H), 1.31 (t, J = 7.3 Hz, 3H). ^{13}C NMR (100 MHz, DMSO-d_6) δ 179.19, 159.95, 157.33, 154.43, 142.66, 134.39, 112.06, 94.19, 78.88, 75.88, 54.29, 44.83, 41.21, 39.73, 26.04, 13.68. HRMS (ESI): m/z calcd $C_{16}H_{21}N_7S$ $[M+H]^+$ 344.1613, found 344.1657. HPLC purity: 99.0%.

4.1.7.3. 1-Ethyl-3-(6-(4-(3-(prop-2-yn-1-yl)amino)propyl)-1H-imidazol-1-yl) pyrimidin-4-yl)thiourea (***3a***). Yellow solid, 65% yield. Mp 118−120 °C; ^{1}H NMR (400 MHz, DMSO-d_6) δ 11.19 (t, J = 5.3 Hz, 1H), 10.92 (s, 1H), 8.73 (s, 1H), 8.35 (d, J = 1.1 Hz, 1H), 7.41 (d, J = 15.7 Hz, 1H), 7.24 (s, 1H), 3.68–3.59 (m, 2H), 3.30 (d, J = 2.3 Hz, 2H), 3.03 (t, J = 2.3 Hz, 1H), 2.62–2.52 (m, 4H), 1.78–1.68 (m, 2H), 1.22 (t, J = 7.2 Hz, 3H). ^{13}C NMR (100 MHz, DMSO-d_6) δ 179.20, 159.96, 157.32, 154.45, 144.41, 134.53, 111.57, 94.17, 82.72, 73.79, 47.30, 39.73, 37.28, 28.28, 25.48, 13.69. HRMS (EI): m/z calcd $C_{16}H_{21}N_7S$ (M^+) 343.1579, found 343.1573. HPLC purity: 98.3%.

4.1.7.4. 1-Ethyl-3-(6-(4-(3-(methyl(prop-2-yn-1-yl)amino)propyl)-1H-imidazol -1-yl)pyrimidin-4-yl) thiourea (***3b***). Yellow solid, 71% yield. Mp 122−124 °C; ^{1}H NMR (400 MHz, DMSO-d_6) δ 11.19 (t, J = 5.3 Hz, 1H), 10.92 (s, 1H), 8.74 (s, 1H), 8.35 (d, J = 1.1 Hz, 1H), 7.44 (s, 1H), 7.24 (s, 1H), 3.68–3.60 (m, 2H), 3.30 (d, J = 2.3 Hz, 2H), 3.10 (t, J = 2.3 Hz, 1H), 2.56–2.52 (m, 2H), 2.38 (t, J = 7.2 Hz, 2H), 2.19 (s, 3H), 1.80–1.67 (m, 2H), 1.22 (t, J = 7.2 Hz, 3H). ^{13}C NMR (125 MHz, DMSO-d_6) δ 179.20, 159.93, 157.29, 154.45, 144.35, 134.50, 111.57, 94.17, 79.04, 75.63, 54.43, 44.92, 41.24, 39.69, 26.33, 25.41, 13.65. HRMS (EI): m/z calcd $C_{17}H_{23}N_7S$ (M^+) 357.1736, found 357.1739. HPLC purity: 98.5%.

*4.1.8. General synthetic procedure for **2d-c***

To a solution of compound **2a** (164 mg, 0.5 mmol) in CH_3CN (8 mL), corresponding RX (0.55 mmol), Et_3N (101 mg, 1 mmol), and a catalytic amount of KI were added. The reaction mixture was refluxed for 12 h, and the solvent was evaporated to dryness under reduced pressure. The residue was purified on a silica gel column using mixtures of MeOH:CH_2Cl_2 as the eluent, affording the target

compounds **2c-d**.

4.1.8.1 1-Ethyl-3-(6-(4-(2-(ethyl(prop-2-yn-1-yl)amino)ethyl)-1H-imidazol-1-yl) pyrimidin-4-yl)thiourea (***2c***). Iodoethane was used as the corresponding RX. White solid, 33% yield. Mp 154−155 °C; ^{1}H NMR (400 MHz, CD_3OD) δ 8.72 (s, 1H), 8.54 (s, 1H), 7.70 (s, 1H), 7.02 (s, 1H), 3.75 (q, *J* = 7.3 Hz, 2H), 3.71 (d, *J* = 1.8 Hz, 2H), 3.10 – 3.04 (m, 2H), 2.93 – 2.84 (m, 4H), 2.83 (s, 1H), 1.32 – 1.30 (m, 3H), 1.20 (t, *J* = 7.2 Hz, 3H). ^{13}C NMR (125 MHz, DMSO-d_6) δ 179.18, 159.96, 157.35, 154.43, 134.49, 112.22, 94.22, 51.87, 46.93, 40.70, 40.11, 29.02, 13.68. HRMS (EI): *m*/*z* calcd $C_{17}H_{23}N_7S$ (M^+) 357.1736, found 357.1738. HPLC purity: 97.5%.

4.1.8.2. 1-(6-(4-(2-((Cyanomethyl)(prop-2-yn-1-yl)amino)ethyl)-1H-imidazol-1 -yl)pyrimidin-4-yl)-3-ethylthiourea (***2d***). 2-Bromoacetonitrile was used as the corresponding RX. White solid, 35% yield. Mp 159−160°C; ^{1}H NMR (400 MHz, DMSO-d_6) δ 11.19 (t, *J* = 5.3 Hz, 1H), 10.95 (s, 1H), 8.74 (s, 1H), 8.36 (d, *J* = 1.3 Hz, 1H), 7.52 (s, 1H), 7.25 (s, 1H), 3.84 (s, 2H), 3.68–3.59 (m, 2H), 3.45 (d, *J* = 2.4 Hz, 2H), 3.30 (t, *J* = 2.4 Hz, 1H), 2.86–2.80 (m, 2H), 2.77–2.71 (m, 2H), 1.22 (t, *J* = 7.2 Hz, 3H). ^{13}C NMR (100 MHz, DMSO-d_6) δ 179.20, 159.98, 157.37, 154.45, 141.97, 134.58, 116.14, 112.34, 94.27, 78.43, 76.69, 51.74, 42.57, 41.21, 39.73, 25.70, 13.70. HRMS (EI): *m*/*z* calcd $C_{17}H_{20}N_8S$ (M^+) 368.1532, found 368.1515. HPLC purity: 95.8%.

4.2. Biological activity

4.2.1. In vitro inhibition of AChE and BuChE

The enzyme inhibition activity of the tested compounds was performed using the method of Ellman et al. with slight modification [44]. The rat cortex was homogenized in cold 75 mM sodium phosphate buffer (pH 7.4) as the AChE source, and the rat serum was collected as the BuChE source. 5,5′-dithiobis (2-nitrobenzoic acid) (DTNB), acetylthiocholine iodide and butyrylthiocholine iodide were purchased from Sigma. Huperzine A (Hup A) was used as reference compound. 1 μL of the tested compounds with an appropriate concentration (1 nM to 10 mM) was added into the assay solution, which consisted of 50 μL of 0.1 M phosphate buffer, 50 μL of 0.2% DTNB, 109 or 99 μL of deionized water, 10 μL of rat cortex homogenate or 20

μL of rat serum, and 30 μL of 2 mM acetylthiocholine iodide or 40 μL of 2 mM butyrylthiocholine iodide as the substrate of the AChE or BuChE enzymatic reaction, respectively. Then the mixture was incubated for 20 min at room temperature. The production of the yellow anion of 5-thio-2-nitrobenzoic acid was measured with a microplate reader (DTX 880, Beckman Coulter) at 450 nm. The inhibition percentage caused by the presence of test compound was calculated, and the IC_{50} was defined as the concentration of the compound that reduced 50% of the enzymatic activity without inhibitor.

4.2.2. In vitro inhibition of hMAO-A and hMAO-B

MAO kit purchased from Invtrogen Company was used to evaluate the inhibitory activity for recombinant human MAOs of the target compounds. hMAO-A and hMAO-B (Sigma) were dilute to 12.5 μg/mL and 75 μg/mL using 1×buffer, respectively. Compounds were dissolved in DMSO (10 mM) and diluted in 50 mM KH_2PO_4 buffer (pH 7.4) to the desired final concentration. All the compounds are soluble at the tested concentration. Test drugs (50 μL) and MAOs (50 μL) were incubated at 37°C for 15 min in a 96-well costar plate. Amplex Red reagent working solution (100 μL), which consisted of 2 mM p-tyramine for hMAO-A or benzylamine for hMAO-B, 2 U/mL horseradish peroxide, and 200 mM Amplex Red reagent, was added into the mixture to start the reaction. After 15 min of incubation at 37 °C, the generated fluorescence was recorded by Molecular Devices (SpectraMax i3; excitation, 545 nm; emission, 590 nm). The specific fluorescence emission was calculated after subtraction of the background activity. The background activity was determined from wells containing all components except the MAO isoforms, which were replaced by a sodium phosphate buffer solution. The percent inhibition was calculated by the following expression:

$$\text{Inhibitition\%} = [1 - (F_i - F_{blank}) / (F_{control} - F_{blank})] \times 100\%$$

Where F_i is the fluorescence of the compounds; $F_{control}$ is the fluorescence of the control group; F_{blank} is the fluorescence of background.

4.2.3. Oxygen radical absorbance capacity (ORAC-FL) assay

Compounds were dissolved in DMSO (10 mM) and diluted with 75 mM phosphate buffer (pH 7.4) to 20 μM. Fuorescein (FL) stock solution and 2,2′-azobis(amidinopropane) dihydrochloride (AAPH) were prepared and diluted with 75 mM phosphate buffer (pH 7.4) to 0.117 μM and 40 mM, respectively. A solution of (±)-6-hydroxy-2,5,7,8-tetramethylchroman2-carboxylic acid (Trolox) was diluted with the same buffer to 100, 80, 60, 50, 40, 20, and 10 μM. The mixture of the tested compounds (20 μL) and FL (120 μL) was incubated for 10 min at 37 °C, and then 60 μL of the AAPH solution was added. The fluorescence was recorded by Molecular Devices every two minutes for 180 min (SpectraMax i3; excitation, 485 nm; emission, 535 nm). A blank was determined using phosphate buffer instead of the tested compounds. All reaction mixtures were prepared in triplicate, and at least three independent runs were performed for each sample. The area under the fluorescence decay curve (AUC) after subtraction of the curve of the blank was calculated using the following equation:

$$\mathrm{AUC} = 1 + \sum_{i=1}^{i=180} f_i/f_0$$

In which f_0 is the initial fluorescence reading at 0 min and f_i is the fluorescence reading at time *i*. The net AUC was calculated by the expression $\mathrm{AUC_{sample}} - \mathrm{AUC_{blank}}$. The ORAC value for each sample were expressed as Trolox equivalents calculated from the ratio of the slopes of the concentration-response curves, the antioxidant *vs* Trolox.

4.2.4. Metal-chelating study

The chelating studies were performed with a UV−vis spectrophotometer at wavelengths ranging from 200 to 500 nm. The absorption spectra of compound **1b** (40 μM, final concentration) alone or in the presence of $CuCl_2$, $FeSO_4$, $FeCl_3$, or $ZnCl_2$ (20 μM, final concentration) for 30 min in buffer (20 mM HEPES, 150 mM NaCl, pH 7.4) were recorded at room temperature.

4.2.5. Inhibition of ROS produced by copper redox cycling

The tested compounds were dissolved in methanol and diluted with PBS buffer (20 mM, containing NaCl 100 mM, pH 7.4) to the desired final concentration. The

other solutions, except $CuSO_4$ (dissolved in water and diluted in PBS), were mixed and diluted in the same PBS buffer with a final sample volume of 200 μL (ligand [15 μM] or PBS, Cu(II) [5 μM], deferoxamine [1 μM], CCA [50 μM], and then ascorbate [150 μM]). Each experiment was performed in triplicate. Hydroxyl radical production was measured as the conversion of CCA into 7-hydroxy-CCA by Molecular Devices at 37 °C (SpectraMax i3; excitation, 395 nm; emission, 450 nm). All of the test solutions contained 0.1% methanol.

4.2.6. Dot blot assay

Aβ_{1-42} (Sigma, CA, U.S.) was dissolved in ammonium hydroxide (1% v/v) to afford a stock solution (2000 μM), and stored at −80 °C. For the experiments, the Aβ_{1-42} stock solution was diluted in 20 μM HEPES (pH 6.6) with 150 μM NaCl. The mixture of the peptide (25 μM, final concentration) with or without Cu(II) (25 μM, final concentration) and the tested compound (50 μM, final concentration) was incubated at 37 °C for 24 h. For the dot immunoblot assay, each Aβ sample was spotted (5 μL) on nitrocellulose membranes (GE Healthcare). Afterward, the membranes were blocked by 5% nonfat milk for 1 h and probed with A11 (Millipore) or 6E10 (Convance) antibodies at 4 °C overnight. The blots were washed with TBST and incubated with suitable horseradish peroxidase-conjugated secondary antibodies at room temperature for 1 h. Images were acquired by an image system (Tanon) and were analyzed using image J software.

4.2.7. TEM assay [50, 51].

In this experiment, experimental method was the same as the dot blot assay: The Aβ_{1-42} stock solution was diluted with the same HEPES, and the mixture of Aβ (25 μM) solutions, ± $CuCl_2$ (25 μM), ± compounds (50 μM) were incubated for 24 h at 37 °C. Aliquots (10 μL) of the samples were placed on a carbon-coated copper grid for 30 min. Each grid was stained with phosphotungstic acid (2%, 10 μL) for 20 s. After draining the excess staining solution, the specimen was transferred for imaging by transmission electron microscopy (JEM-1400). All compounds were solubilized in the bu□er used for the experiment.

4.2.8. Cell viability assay

Primary cortical neurons (PCNs) were isolated from E17 SD rat embryos as described. Briefly, cortices were dissected in old high glucose Dulbecco's Modified Eagle's Medium (HG-DMEM, Invitrogen) and dissociated into single cells by trypsinization. Cells were seeded into 96-well plates coated with poly-L-lysine at a density of 3×10^4 cells per well. PCNs were cultured in a neurobasal medium (Invitrogen) containing 0.5 mM L-glutamine , 2% B27 supplement, penicillin (60 mg/L) and streptomycin (50 mg/L). Half of the culture medium was refreshed every 3 days. The following experiments were performed at 9 days of culture [52]. For the neurotoxicity test, the cells were treated with compounds at 10 μM, 30 μM, and 100 μM for 24 h. 3-(4,5-dimethylthiazol-2-yl)-2,5-diphenyltetrazolium bromide (MTT, Sangon Biotech, China) analysis was performed to measure the cell viability. A total of 10 μL of MTT (5 mg/mL) was added into each well and incubated at 37 °C for 4 h. The production of MTT formazan was determined by measuring the absorbance at 490 nm. The cell viability was calculated and presented by the percentage of vehicle-treated group.

For neuroprotection of compound **1b** on Cu^{2+}-induced A$\beta_{1\text{-}42}$ neurotoxic model, the preparation of the A$\beta_{1\text{-}42}$ sample was the same as that for the dot blot assay. The A$\beta_{1\text{-}42}$ samples were added into the cell cultures at a concentration of 1 μM for 24 h. Then, the cell viability was measured by the MTT assay and normalized by the vehicle group.

4.2.9. In vitro blood−brain barrier permeation assay

Brain penetration of compounds was evaluated using a parallel artificial membrane permeation assay (PAMPA), in a similar manner as described by Di et al [49]. Commercial drugs were purchased from Sigma and Alfa Aesar. The porcine brain lipid (PBL) was obtained from Avanti Polar Lipids. The donor microplate (PVDF membrane, pore size 0.45 mm) and the acceptor microplate were both from Millipore. The 96-well UV plate was from Corning Incorporated. The acceptor 96-well microplate was filled with 300 μL of PBS:EtOH (7:3, v:v), and the filter membrane was impregnated with 4 μL of PBL in dodecane (20 mg mL^{-1}).

Compounds were dissolved in DMSO at 5 mg mL^{-1} and diluted to 100 μg mL^{-1} with PBS:EtOH (7:3, v:v), then 200 μL was added to the donor wells. The acceptor filter plate was carefully placed on the donor plate to form a sandwich, which was left undisturbed for 12 h at 25 °C. After incubation, the donor plate was carefully removed and the concentration of compounds in the acceptor wells was determined using a UV plate reader (SpectraMax i3). Each sample was analyzed at eight wavelengths, in four wells, in at least three independent runs, and the results are given as the mean ± standard deviation. P_e was calculated using the following equation:

$$P_e = -\left(\frac{V_d \times V_a}{(V_d + V_a)\ A \times t}\right) \times \ln\left(1 - \frac{[drug]_{acceptor}}{[drug]_{equilibrium}}\right)$$

where V_d is the volume in the donor well, V_a is the volume in the acceptor well, A is the filter area, t is the permeation time, $[drug]_{acceptor}$ is the absorbance of the compound in the acceptor well, and $[drug]_{equilibrium}$ is the theoretical equilibrium absorbance.

In the experiment, 13 quality control standards of known BBB permeability were included to validate the analysis set (**Table S1**, *Supporting Information*). A plot of the experimental data versus reference values gave a strong linear correlation, P_e (exp.) = 0.974P_e (lit.) – 0.8152 (R^2 = 0.9651) (**Fig. S2**, *Supporting Information*). From this equation and the limit established by Di et al. for blood−brain barrier permeation, we concluded that compounds with permeability greater than 3.08 × 10^{-6} cm s^{-1} could cross the blood−brain barrier and P_e values from 1.13×10^{-6} cm s^{-1} to 3.08 × 10^{-6} cm s^{-1} were classified as "CNS±" (BBB permeation uncertain) (**Table S2**, *Supporting Information*).

4.2.10. Cognitive performance evaluation

Imprinting control region (ICR) mice weighing 18−25 g were obtained from the Laboratory Animal Center, Chinese Academy of Sciences (Shanghai, China). All procedures were carried out in compliance with the National Institutes of Health Guide for the Care and Use of Laboratory Animals, as well as the guidelines of the Animal Care and Use Committee of Shanghai Institute of Materia Medica. The mice were trained to find the platform in a rectangular plastic channel water maze (80 cm ×

50 cm × 20 cm), which was described in detail in our previous study [53]. Each mouse received at least two training sessions daily for four consecutive days before testing with the criterion of finding the platform within 30 s and committing less than three errors of entering no-exit paths. Mice that met the criterion were randomly divided into four treatment groups (N = 16): control (Ctrl, saline-treated) group, scopolamine (Scop) group, scopolamine (Scop) + huperzine A (Hup A) group, and scopolamine (Scop) + **1b·HCl** group. To evaluate the cognitive-enhancing effect of compound **1b·HCl** on scopolamine-induced cognitive impairment, scopolamine (4.5 mg/kg) was injected (i.p.) 20 min before the behavior test, and compound **1b·HCl** (30 mg/kg) or positive control (Hup A, 0.1 mg/kg) was administered (i.g.) 40 min prior to the administration of scopolamine. The escape latency and number of errors were recorded.

4.3. Molecular Docking Studies

The simulation systems were built based on structures retrieved from the Protein Data Bank (PDB: 2V60 for hMAO-B, 5EIE for mAChE). For proteins, heteroatoms and water molecules were removed and hydrogen atoms were assigned using Protein Preparation Wizard. For ligand **1b**, LigPrep was used to produce the structure of optimum energy. Docking simulations were performed using Glide in Schrödinger software [54].

Supplementary data

Supplementary data include the synthesis of intermediate **4c**, compound **1b·HCl**, ThT fluorescence assay, raw data of the *in vitro* blood-brain barrier permeation assay and the NMR spectra of intermediates and final compounds.

Acknowledgments

Financial support for this research was provided by the National Natural Science Foundation of China (Grants 21672064, 21372001, 81522045), Yang-Fan Program from the Science and Technology Commission of Shanghai (Grants 17YF1403600), and the Fundamental Research Funds for the Central Universities.

Abbreviations used

AD, Alzheimer’s disease; AChE, acetylcholinesterase; BuChE, butyrylcholinesterase; ACh, acetylcholine; AChEIs, AChE inhibitors; MAOs, monoamine oxidases; MAO-A, monoamine oxidase A; MAO-B, monoamine oxidase B; CAS catalytic active site; FAD, flavin adenine dinucleotide; Aβ, beta amyloid protein; BBB, blood−brain barrier; Hup A, huperzine A; CFDA, China Food and Drug Administration; ROS, reactive oxygen species; MTDLs, multitarget-directed ligands; ChEs, cholinesterases; SAR, structure activity relationship; rChE, rat cholinesterase; hMAO-A, human monoamine oxidase A; hMAO-B, human monoamine oxidase B; ORAC, free oxygen radical absorbance capacity; AAPH, 2,2'-azobis-(amidinopropane)dihydrochloride; EDTA, ethylenediaminetetraacetic acid; EGCG, epigallocatechin gallate; CCA, coumarin-3-carboxylic acid; CQ, Clioquinol; TEM, transmission electron microscopy; ThT thioflavine T; MTT, 3-(4,5-dimethylthiazol-2-yl)-2,5-diphenyltetrazolium bromide; PCN, primary cortical neuron; Don, donepezil; PAMPA, parallel artificial membrane permeation assay; mAChE, mice acetylcholinesterase; MP, melting point; TLC, thin-layer chromatography; LC-MS/MS, liquid chromatography tandem mass spectrometry; DTNB, 5,5′-dithiobis (2-nitrobenzoic acid); HEPES, 2-[4-(2-hydroxyethyl)piperazin-1-yl] ethanesulfonic acid; PBS, phosphate buffer salt. PBL, porcine brain lipid.

References

[1] A.S. Association, Alzheimer's disease facts and figures, Alzheimer's Dementia 9 (2013) 208–245.

[2] M. Goedert, M.G. Spillantini, A Century of Alzheimer's Disease, Science 314 (2006) 777–781.

[3] Alzheimer's Disease International, World Alzheimer Report. http://www.alz.co.uk/research/files/WorldAlzheimerReport2015ExecutiveSummary.pdf (accessed April 24, 2016).

[4] V.N. Talesa, Acetylcholinesterase in Alzheimer's disease, Mech. Ageing Dev. 122 (2001) 1961–1969.

[5] J. Hardy, D.J. Selkoe, The Amyloid Hypothesis of Alzheimer's Disease: Progress

and Problems on the Road to Therapeutics, Science 297 (2002) 353–356.

[6] J. Hardy, Alzheimer's disease: the amyloid cascade hypothesis: an update and reappraisal, J. Alzheimer's Dis. 9 (2006) 151–153.

[7] K.J. Barnham, C.L. Masters, A.I. Bush, Neurodegenerative diseases and oxidative stress, Nat. Rev. Drug Discovery 3 (2004) 205–214.

[8] M.L. Hegde, P. Bharathi, A. Suram, C. Venugopal, R. Jagannathan, P. Poddar, P. Srinivas, K. Sambamurti, K.J. Rao, J. Scancar, L. Messori, L. Zecca, P. Zatta, Challenges Associated with Metal Chelation Therapy in Alzheimer's Disease, J. Alzheimer's Dis. 17 (2009) 457–468.

[9] S. Bolognin, D. Drago, L. Messori, P. Zatta, Chelation therapy for neurodegenerative diseases, Med. Res. Rev. 29 (2009) 547–570.

[10] P.T. Francis, A.M. Palmer, M. Snape, G.K. Wilcock, The cholinergic hypothesis of Alzheimer's disease: a review of progress, J. Neurol., Neurosurg. Psychiatry 66 (1999) 137–147.

[11] K.D. Green, M. Fridman, S. Garneautsodikova, hChAT: a tool for the chemoenzymatic generation of potential acetyl/butyrylcholinesterase inhibitors. ChemBioChem 10 (2009) 2191–2194.

[12] Q. Xie, H. Wang, Z. Xia, M. Lu, W. Zhang, X. Wang, W. Fu, Y. Tang, W. Sheng, W. Li, W. Zhou, X. Zhu, Z. Qiu, H. Chen, Bis-(-)-nor-meptazinols as novel nanomolar cholinesterase inhibitors with high inhibitory potency on amyloid-beta aggregation, J. Med. Chem. 51 (2008) 2027–2036.

[13] D. Munoz-Torrero, Acetylcholinesterase inhibitors as disease-modifying therapies for Alzheimer's disease, Curr. Med. Chem. 15 (2008) 2433–2455.

[14] P. Anand, B. Singh, A review on cholinesterase inhibitors for Alzheimer's disease, Arch. Pharmacal Res. 36 (2013) 375–399.

[15] D. Lo, G.T. Grossberg, Use of memantine for the treatment of dementia, Expert Rev. Neurother. 11 (2011) 1359–1370.

[16] A. Takeda, E. Loveman, A. Clegg, J. Kirby, J. Picot, E. Payne, C. Green, A systematic review of the clinical effectiveness of donepezil, rivastigmine and galantamine on cognition, quality of life and adverse events in Alzheimer's

disease, Int. J. Geriatr. Psychopharmacol. 21 (2006) 17–28.

[17] P. Raina, P. Santaguida, A. Ismaila, C. Patterson, D. Cowan, M. Levine, L. Booker, M. Oremus, Effectiveness of Cholinesterase Inhibitors and Memantine for Treating Dementia: Evidence Review for a Clinical Practice Guideline, Ann. Intern. Med. 148 (2008) 379–397.

[18] J.C. Shih, K. Chen, M.J. Ridd, Monoamine oxidase: from genes to behavior, Annu. Rev. Neurosci. 22 (1999) 197–217.

[19] G.D. Mellick, D.D. Buchanan, S.J. Mccann, K.M. James, A.G. Johnson, D.R. Davis, N. Liyou, D. Chan, D.G Le-Couteur, Variations in the monoamine oxidase B (MAOB) gene are associated with Parkinson's disease, Mov. Disord. 14(2) (1999) 219–24.

[20] D.E. Edmondson, A. Mattevi, C. Binda, M. Li, F. Hubaleka, Structure and mechanism of monoamineoxidase, Curr. Med. Chem. 11 (2004) 1983–1993.

[21] J. Wouters, Structural aspects of monoamine oxidase and its reversible inhibition, Curr. Med. Chem. 5 (1998) 137–162.

[22] M.B.H. Youdim, D. Edmondson, K.F. Tipton, The therapeutic potential of monoamine oxidase inhibitors, Nat. Rev. Neurosci. 7 (2006) 295–309.

[23] R. Adolfsson, C.G. Gottfries, L. Oreland, A. Wiberg, B. Winblad. Increased activity of brain and platelet monoamine oxidase in dementia of Alzheimer type. Life Sci. 27 (1980) 1029–1034.

[24] P. Riederer, W. Danielczyk, E. Grunblatt, Monoamine oxidase-B inhibition in Alzheimer’s disease. Neurotoxicology 25 (2004) 271–277.

[25] F. Chimenti, D. Secci, A. Bolasco, P. Chimenti, B. Bizzarri, A. Granese, S. Carradori, M. Yanez, F. Orallo, S. Alcaro, Synthesis, Molecular Modeling, and Selective Inhibitory Activity against Human Monoamine Oxidases of 3-Carboxamido-7-Substituted Coumarins, J. Med. Chem. 52 (2009) 1935–1942.

[26] M.J. Matos, C. Teran, Y. Perez-Castillo, E. Uriarte, L. Santana, D. Vina, Synthesis and study of a series of 3-arylcoumarins as potent and selective monoamine oxidase B inhibitors, J. Med. Chem. 54 (2011) 7127–7137.

[27] O. Bar-Am, T. Amit, O. Weinreb, M.B. Youdim, S. Mandel, Propargylamine

containing compounds as modulators of proteolytic cleavage of amyloid-beta protein precursor: involvement of MAPK and PKC activation, J. Alzheimer's Dis. 21 (2010) 361–371.

[28] H.J. Lee, K.J. Korshavn, A. Kochi, J.S. Derrick, M.H. Lim, Cholesterol and metal ions in Alzheimer's disease, Chem. Soc. Rev. 43 (2014) 6672–6682.

[29] F. Molina-Holgado, R.C. Hider, A. Gaeta, R. Williams, P. Francis, Metals ions and neurodegeneration, BioMetals 20 (2007) 639–654.

[30] C.D. Syme, R.C. Nadal, S.E.J. Rigby, J.H. Viles, Copper Binding to the Amyloid-β (Aβ) Peptide Associated with Alzheimer's Disease, J. Biol. Chem. 279 (2004) 18169–18177.

[31] C. Hureau, P. Faller, Abeta-mediated ROS production by Cu ions: structural insights, mechanisms and relevance to Alzheimer's disease, Biochimie 91 (2009) 1212–1217.

[32] R.A. Himes, G.Y. Park, G.S. Siluvai, N.J. Blackburn, K.D. Karlin, Structural Studies of Copper(I) Complexes of Amyloid-β Peptide Fragments: Formation of Two-Coordinate Bis(histidine) Complexes, Angew. Chem., Int. Ed. 47 (2008) 9084–9087.

[33] S.S. Hindo, A.M. Mancino, J.J. Braymer, Y. Liu, S. Vivekanandan, A. Ramamoorthy, M.H. Lim, Small molecule modulators of copper-induced Abeta aggregation, J. Am. Chem. Soc. 131 (2009) 16663–16665.

[34] C. Rodriguez-Rodriguez, M. Telpoukhovskaia, C. Orvig, The art of building multifunctional metal-binding agents from basic molecular scaffolds for the potential application in neurodegenerative diseases, Coord. Chem. Rev. 256 (2012) 2308–2332.

[35] D. Pratico, Oxidative stress hypothesis in Alzheimer's disease: a reappraisal, Trends Pharmacol. Sci. 29 (2008) 609–615.

[36] H.P. Lee, X. Zhu, G. Casadesus, R.J. Castellani, A. Nunomura, M.A. Smith, H.G. Lee, G. Perry, Antioxidant approaches for the treatment of Alzheimer's disease, Expert Rev. Neurother. 10 (2010) 1201–1208.

[37] A. Cavalli, M.L. Bolognesi, A. Minarini, M. Rosini, V. Tumiatti, M. Recanatini,

C. Melchiorre, Multi-target-Directed Ligands To Combat Neurodegenerative Diseases, J. Med. Chem. 51 (2008) 347–372.

[38] Z. Wang, Y. Wang, B. Wang, W. Li, L. Huang, X. Li, Design, Synthesis and Evaluation of Orally Available Clioquinol-Moracin M Hybrids as MultiTarget-Directed Ligands for Cognitive Improvement in a Rat Model of Neurodegeneration in Alzheimer's Disease, J. Med. Chem. 58 (2015) 8616–8637.

[39] M.B.H. Youdim, T. Amit, O. Bar-Am, O. Weinreb, M. Yogev-Falach, Implications of co-morbidity for etiology and treatment of neurodegenerative diseases with multifunctional neuroprotective-neurorescue drugs: ladostigil, Neurotoxic. Res. 10 (2006) 181–192.

[40] J. Sterling, Y. Herzig, T. Goren, N. Finkelstein, D. Lerner, W. Goldenberg, I. Miskolczi, S. Molnar, F. Rantal, T. Tamas, G. Toth, A. Zagyva, A. Zekany, G. Lavian, A. Gross, R. Friedman, M. Razin, W. Huang, B. Krais, M. Chorev, M.B. Youdim, M. Weinstock, Novel Dual Inhibitors of AChE and MAO Derived from Hydroxy Aminoindan and Phenethylamine as Potential Treatment for Alzheimer's Disease, J. Med. Chem. 45 (2002) 5260–5279.

[41] C. Lu, Q. Zhou, J. Yan, Z. Du, L. Huang, X. Li, A novel series of tacrine-selegiline hybrids with cholinesterase and monoamine oxidase inhibition activities for the treatment of Alzheimer's disease, Eur. J. Med. Chem. 62 (2013) 745–753.

[42] X. Li, H. Wang, Z. Lu, X. Zheng, W. Ni, J. Zhu, Y. Fu, F. Lian, N. Zhang, J. Li, H. Zhang, F. Mao, Development of Multifunctional Pyrimidinylthiourea Derivatives as Potential Anti-Alzheimer Agents, J. Med. Chem. 59 (2016) 8326–8344.

[43] G. Bazzu, G. Rocchitta, R. Migheli, M.D. Alvau, M. Zinellu, G. Puggioni, G. Calia, G. Mercanti, P. Giusti, M.S. Desole, P.A. Serra, Effects of the neurotoxin MPTP and pargyline protection on extracellular energy metabolites and dopamine levels in the striatum of freely moving rats, Brain Res. 1538 (2013) 159–171.

[44] G.L. Ellman, K.D. Courtney, V.J. Andres, R.M. Featherstone, A new and rapid colorimetric determination of acetylcholinesterase activity, Biochem. Pharmacol.

(Amsterdam, Neth.) 7 (1961) 88–90.

[45] X. Huang, C.S. Atwood, M.A. Hartshorn, G. Multhaup, L.E. Goldstein, R.C. Scarpa, M.P. Cuajungco, D.N. Gray, J. Lim, R.D. Moir, R.E. Tanzi, A.I. Bush, The Aβ Peptide of Alzheimer's Disease Directly Produces Hydrogen Peroxide through Metal Ion Reduction, Biochemistry 38 (1999) 7609–7616.

[46] A. Davalos, C. Gomez-Cordoves, B. Bartolome, Extending Applicability of the Oxygen Radical Absorbance Capacity (ORAC−Fluorescein) Assay, J. Agric. Food Chem. 52 (2004) 48–54.

[47] B. Ou, M. Hampsch-Woodill, R.L. Prior, Development and Validation of an Improved Oxygen Radical Absorbance Capacity Assay Using Fluorescein as the Fluorescent Probe, J. Agric. Food Chem. 49 (2001) 4619–4626.

[48] L. Guilloreau, S. Combalbert, A. Sournia-Saquet, H. Mazarguil, P. Faller, Redox chemistry of copper-amyloid-beta: the generation of hydroxyl radical in the presence of ascorbate is linked to redox-potentials and aggregation state, ChemBioChem 8 (2007) 1317–1325.

[49] L. Di, E.H. Kerns, K. Fan, O.J. Mcconnell, G.T. Carter, High throughput artificial membrane permeability assay for blood–brain barrier, Eur. J. Med. Chem. 38 (2003) 223–232.

[50] J.S. Choi, J.J. Braymer, R.P.R. Nanga, A. Ramamoorthy, M.H. Lim, Design of small molecules that target metal-Aβ species and regulate metal-induced Aβ aggregation and neurotoxicity, Proc. Natl. Acad. Sci. U. S. A. 107 (2010) 21990–21995.

[51] F. Mao, J. Yan, J. Li, X. Jia, H. Miao, Y. Sun, L. Huang, X. Li, New multi-target-directed small molecules against Alzheimer's disease: a combination of resveratrol and clioquinol, Org. Biomol. Chem. 12 (2014) 5936–5944.

[52] J. Du, L. Feng, F. Yang, B. Lu, Activity- and Ca^{2+}-dependent modulation of surface expression of brain-derived neurotrophic factor receptors in hippocampal neurons, J. Cell Biol. 150 (2000) 1423–1433.

[53] J. Liu, H. Zhang, X. Tang, B, Wang, X. He, D. Bai, Effects of synthetic (-)-huperzine A on cholinesterase activities and mouse water maze performance,

Acta Pharmacol. Sin. 19 (1998) 413–416.

[54] Schrödinger Suite; Schrödinger, LLC, New York, 2016.

- Novel compounds with good multifunctional anti-AD activities were discovered.
- Compound **1b** showed potential druggability: low cytotoxicity and BBB permeability.
- Compound **1b** ameliorated scopolamine-induced cognitive impairment in mice.